NACA RM E9K25

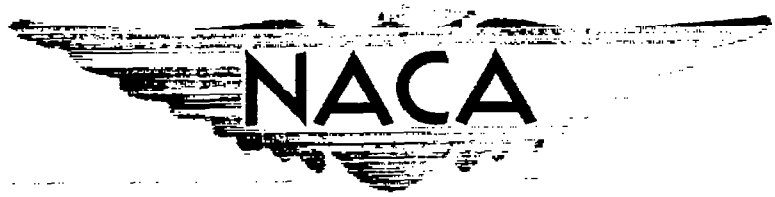

RESEARCH MEMORANDUM

STUDY OF FLOW CONDITIONS AND DEFLECTION ANGLE AT EXIT OF TWO-DIMENSIONAL CASCADE OF TURBINE ROTOR BLADES AT CRITICAL AND SUPERCRITICAL PRESSURE RATIOS

By Cavour H. Hauser, Henry W. Plohr
and Gerhard Sonder

Lewis Flight Propulsion Laboratory
Cleveland, Ohio

TECHNICAL EDITING WAIVED

NATIONAL ADVISORY COMMITTEE FOR AERONAUTICS

WASHINGTON
March 10, 1950

NACA RM E9K25

NATIONAL ADVISORY COMMITTEE FOR AERONAUTICS

RESEARCH MEMORANDUM

STUDY OF FLOW CONDITIONS AND DEFLECTION ANGLE AT EXIT OF TWO-DIMENSIONAL CASCADE OF TURBINE ROTOR BLADES AT CRITICAL AND SUPERCRITICAL PRESSURE RATIOS

By Cavour H. Hauser, Henry W. Plohr
and Gerhard Sonder

SUMMARY

An analysis was made of the flow conditions downstream of a cascade of turbine rotor blades at critical and supercritical pressure ratios. The results of five theoretical methods for determining the deflection angle are compared with those of an experimental method using the conservation-of-momentum principle and static-pressure surveys, and also are compared with an analysis of schlieren photographs of the flow downstream of the blades. A two-dimensional cascade of six blades with an axial width of 1.80 inches was used for the static-pressure surveys and for some of the schlieren photographs. In order to determine the flow conditions several blade chords downstream of the cascade, schlieren photographs were taken of the flow through a cascade of 18 blades having an axial width of 0.60 inch.

For the blade design studied, even at static-to-total pressure ratios considerably lower than that required to give critical velocity at the throat section, the flow was deflected in the tangential direction as predicted for the incompressible case. As the pressure ratio was lowered further, the aerodynamic loading of the rear portion of the blade reached a maximum value and remained constant. After this condition was attained, the expansion downstream of the cascade took place with a constant tangential velocity so that no further increase in the amount of turning across the blade row and no further increase in the loading of the blade was available.

Although none of the five methods for analytically determining the jet-deflection angle gave results that agreed closely with the experimental results, the assumption of nonisentropic expansion with a constant value of tangential velocity after the aerodynamic loading of the rear portion of the blade reached its maximum value gave

the best agreement between theory and experiment. When the entire field of flow a short distance downstream of the blades became supersonic, an end-point condition for which the axial velocity is supersonic was attained, and any further decrease in the pressure ratio did not change the flow conditions at the exit of the blades. The flow for this end-point condition was quantitatively analyzed by the method of characteristics. The deflection of the jet determined by the experimental conservation-of-momentum method was found to remain almost constant at about 7° in the tangential direction until the blade loading reached its maximum value; the deflection angle then changed as the pressure ratio was further decreased, until a maximum value of 15° in the axial direction was obtained for the end-point condition.

INTRODUCTION

In evaluating the performance of a gas turbine, account must be taken of the deflection of the flow from the blade angle at the exit of each row of blades for subsonic and supersonic velocities. For subonsic flow out of blade rows having a reasonably high degree of guidance and solidity, the deviation between the angle of flow and the blade angle at the exit can be approximated by a simple empirical rule (references 1 and 2). When the ratio of the exit static to the inlet total pressure across the blade row is less than the critical value, however, expansion to supersonic velocities takes place and either a complex flow pattern of mixed subsonic and supersonic velocities or a region of completely supersonic velocities is obtained downstream of the blade row. Several theoretical methods for predicting the angle of flow deflection for this condition have been suggested; they are based, however, on different simplifying assumptions and give inconsistent results.

Five such theoretical methods for determining the deflection angle are presented herein and compared with the results of an experimental investigation conducted at the NACA Lewis laboratory of the flow conditions at the exit of a cascade of typical rotor blades. In addition, a detailed analysis of the flow at the exit of the cascade is presented for the conditions examined.

The five theoretical methods evaluated are:

1. Isentropic expansion with constant flow area perpendicular to the axial direction

2. Isentropic expansion with constant tangential velocity

3. Nonisentropic expansion with constant tangential velocity and constant flow area perpendicular to axial direction

4. Isentropic expansion of flow with deflection in axial direction according to Prandtl-Meyer theory of flow around a corner, as derived in reference 3.

5. Evaluation of flow conditions downstream of row of blades by method of characteristics

A two-dimensional cascade was used for the experimental investigation. The blade studied has a solidity of 2.2 based on the axial width and a design reaction of 40 percent with choking flow at the exit. The static-pressure distribution over the peripheral surface of the blade and downstream of the blade row was determined for an inlet temperature of about 600° R, inlet pressures from 20 to 43 pounds per square inch, and static-to-total pressure ratios from 0.60 to 0.16. These static-pressure surveys were used to evaluate the velocity and the flow angle by the conservation-of-momentum principle (impulse law) presented in reference 4. With the blades mounted between glass plates, schlieren photographs of the flow through the passages and in the region downstream of the blades were taken and are presented.

SYMBOLS

The following symbols are used in this report:

A	area, (sq ft)
a	velocity of sound, (ft/sec)
C_p	compression shock wave originating from deflection of flow separated from pressure surface of blade
C_s	compression shock wave originating from delfection of flow separated from suction surface of blade
d	distance across blade channel at exit, (ft)
g	acceleration due to gravity, 32.17 (ft/sec^2)
K	frictional drag force, (lb)

l	flow-path length along suction surface to center of area downstream of throat, (ft)
m	mass flow, (slugs/sec)
P	pressure force, (lb)
p	pressure, (lb/sq ft)
Q and S	arguments used in evaluating Prandtl-Meyer type flow
R	gas constant, 53.34 (ft-lb/(lb)($^{\circ}$R))
Re_l	Reynolds number based on flow-path length l
s	blade pitch or spacing, (ft)
T	absolute temperature, ($^{\circ}$R)
W	relative velocity, (ft/sec)
β	angle of flow measured from tangential direction, (deg)
γ	ratio of specific heats, 1.40 for air
δ	angle of flow deflection, $\beta_4 - \beta_2$, (deg)
θ	blade angle at exit, measured from tangential direction, (deg)
μ	absolute viscosity, ((lb)(sec)/sq ft)
ρ	mass density, (slugs/cu ft)
τ	shearing stress due to boundary-layer friction, (lb/sq ft)

Subscripts:

a	direction of blade suction surface at exit
ac	actual
av	average on suction surface from leading edge to center of area downstream of throat for computing Reynolds number
cr	critical

i	isentropic
n	direction normal to blade suction surface at exit
s	suction surface of blade downstream of throat
t	trailing edge of blade
u	tangential component
x	axial projection or component

Stations:

1	inlet to cascade
2	throat section
3	immediately downstream of cascade where flow is assumed to be deflected in tangential direction to fill wake regions behind blade trailing edge
4	final downstream station where expansion to supercritical conditions is complete
I	first group of static-pressure taps downstream of cascade (See fig. 12.)
II	second group of static-pressure taps downstream of cascade
III	third group of static-pressure taps downstream of cascade
IV	fourth group of static-pressure taps downstream of cascade

Superscripts:

'	stagnation state
$\bar{}$	average value

METHODS FOR DETERMINING JET DEFLECTION AT SUPERCRITICAL PRESSURE RATIOS

For subsonic velocities at the exit of a blade row, numerous investigations (for example, references 1 and 2) have shown that the flow will be deflected from the blade angle θ toward the tangential direction so that the condition of continuity will be satisfied as the stagnant wake region behind the trailing edge of each blade is filled and essentially uniform flow conditions are produced downstream of the blade row. For this condition of uniform subsonic flow, the final flow angle for pressure ratios up to and including the critical pressure ratio is

$$\beta_3 = \sin^{-1} \frac{d}{s} \tag{1}$$

For pressure ratios less than the critical value, however, an expansion to supersonic-flow conditions with deflection in the axial direction will take place.

Six methods of calculating the jet deflection at supercritical pressure ratios are evaluated. The first five methods can be solved when only the blading configuration and the pressure ratio for the expansion downstream of the passage throat are known. In order to apply the sixth method (Stodola's impulse-law method), experimentally determined pressure distributions on the suction surface of the blade near the trailing edge and downstream of the blades must be available.

Method 1: Isentropic expansion with constant flow area perpendicular to axial direction. - A diagram of the flow conditions in the exit region of a blade row for assumed isentropic expansion with constant flow area perpendicular to the axial direction is shown in figure 1. The blade passage is convergent to the throat section (station 2) so that critical-flow conditions are assumed to be attained uniformly over the throat section when the pressure ratio across the blade row is equal to or less than the critical pressure ratio. The flow angle β_2 is assumed to be equal to the blade angle θ. From the continuity relation, if it is assumed that the wakes are completely filled, the final flow angle can be expressed as

$$\beta_4 = \sin^{-1} \left(\frac{\rho_{cr} W_{cr}}{\rho_4 W_4} \right) \left(\frac{d}{s} \right) \tag{2}$$

From isentropic-flow relations, β_4 can be solved if the values of the over-all pressure ratio and the ratio d/s are known. The variation of the supercritical part of the jet deflection $\beta_4 - \beta_3$ with the velocity ratio $(W_4/W_{cr})_i$ is plotted in figure 2 for various values of $\beta_3 = \sin^{-1} d/s$. The total jet deflection is

$$\delta = (\beta_4 - \beta_3) - (\beta_2 - \beta_3)$$

$$= \beta_4 - \beta_2 \tag{3}$$

For each value of the flow angle β_3, the deflection angle increases until the axial velocity at station 4 becomes equal to sonic velocity. The end point on each of the curves corresponds to this condition of choking at station 4. The following relation between the axial and tangential velocities when the axial component is sonic is derived in appendix A:

$$\frac{W_{x,4}}{W_{cr}} = \sqrt{1.0 - \left(\frac{\gamma-1}{\gamma+1}\right)\left(\frac{W_{u,4}}{W_{cr}}\right)^2} \tag{4}$$

The end point of each of the curves in figure 2 was obtained by using isentropic-flow equations and equation (4).

Method 2: Isentropic expansion with constant tangential velocity. - If it is assumed that the tangential components of the force acting on the expanding mass of fluid immediately downstream of the throat of the blade are negligible and that the expansion is isentropic, the conditions of flow at station 4 can be determined. A diagram of flow conditions in the exit region of the blade for these assumptions is shown in figure 3.

The following relations express the flow conditions at station 4. By hypothesis,

$$\frac{W_{u,4}}{W_{cr}} = \frac{W_{u,3}}{W_{cr}} = \cos \beta_3 \tag{5}$$

Isentropic-flow relations determine $(W_4/W_{cr})_i$, and the deflection of the jet is

$$\delta = \cos^{-1}\left(\frac{W_{u,4}}{W_4}\right) - \beta_2 \tag{6}$$

Because all the expansion takes place through an increase in the axial velocity, the flow area $A_{x,4}$ will generally be less than $A_{x,3}$. The area ratio is obtained from the continuity equation,

$$\frac{A_{x,4}}{A_{x,3}} = \frac{1}{\frac{\rho_4 W_{x,4}}{\rho_{cr} W_{cr}}} \sin \beta_3 \tag{7}$$

The supercritical part of the jet-deflection angle $\beta_4 - \beta_3$ is plotted in figure 4 as a function of the blade angle and the ratio of the final velocity to the critical velocity. The variation of the area ratio $A_{x,4}/A_{x,3}$, determined from equation (7), is shown in figure 5. The end points of the curves in figures 4 and 5 correspond to sonic axial velocity at station 4.

Because the conditions at station 4 are assumed to be uniform across the width of the cascade, the required decrease in flow area (fig. 5) could be obtained in the actual turbine only by an increase in the hub-to-tip-diameter ratio downstream of the rotor, which would be an undesirable design condition.

Method 3: Nonisentropic expansion with constant tangential velocity and constant flow area perpendicular to axial direction. - The assumption of constant tangential velocity can be satisfied with constant flow area if the losses between stations 3 and 4 decrease the static density enough to allow continuity of flow with these assumptions.

Figure 6 is obtained through the solution of the equations

$$\left(\frac{W_x}{W_{cr}}\right)^2 + \left(\frac{W_u}{W_{cr}}\right)^2 = \left(\frac{W}{W_{cr}}\right)^2 \tag{8}$$

and

$$\frac{\rho}{\rho'} = \left[1 - \left(\frac{\gamma-1}{\gamma+1}\right)\left(\frac{W}{W_{cr}}\right)^2\right]^{\frac{1}{\gamma-1}} \tag{9}$$

The critical-velocity ratio W/W_{cr} is plotted against the mass-flow parameter $\rho W_x/\rho' W_{cr}$ with contours of constant W_u/W_{cr}.

The curve through the points of maximum value of the mass-flow parameter on each of the contours of constant W_u/W_{cr} corresponds to the choking condition of sonic axial velocity at station 4, which satisfies equation (4).

Because

$$\rho_3 W_{x,3} = \rho_4 W_{x,4} \tag{10}$$

the total-pressure ratio p'_3/p'_4 is

$$\frac{p'_3}{p'_4} = \frac{\left(\frac{\rho W_x}{\rho' W_{cr}}\right)_4}{\left(\frac{\rho W_x}{\rho' W_{cr}}\right)_3} \tag{11}$$

The values of the mass-flow parameters are read from figure 6 at assigned values of the velocity ratios W/W_{cr} and W_u/W_{cr} at stations 3 and 4. The pressure ratio p_4/p'_3 can be obtained from isentropic relations and the relation

$$\frac{p_4}{p'_3} = \frac{\frac{p_4}{p'_4}}{\frac{p'_3}{p'_4}} \tag{12}$$

This method of calculating the jet deflection was not evaluated for the general case, but the solution for the particular blade configuration of the experimental investigation is presented in a subsequent section.

Method 4: Isentropic expansion of flow with deflection in axial direction according to Prandtl-Meyer theory of flow around a corner. - If the primary expansion to the downstream static pressure occurs from the pressure surface of the blade around the tail radius from station 2, as suggested in reference 5, a flow pattern of the Prandtl-Meyer type may occur. Such a flow pattern (fig. 7) is evaluated for an over-all pressure ratio p_4/p'_1 of 0.40. The flow separates from the suction-surface wall, leaving a wide wake region. The deflection of the jet for these conditions is given by the relation (reference 3, pp. 189-197)

$$\delta = \beta_4 - \beta_2 = \frac{1}{2}\left[\sqrt{\frac{\gamma+1}{\gamma-1}}\left(\sin^{-1} Q_2 - \sin^{-1} Q_4\right) + \left(\sin^{-1} S_2 - \sin^{-1} S_4\right)\right] \tag{13}$$

where

$$Q = \gamma - (\gamma-1)\left(\frac{W}{W_{cr}}\right)^2$$

and

$$S = \gamma - (\gamma+1)\frac{1}{(W/W_{cr})^2}$$

The variation of the deflection angle with the ratio of exit velocity to the critical velocity (fig. 8) is evaluated by equation (13). The deflection angle calculated by this method is independent of the blade angle θ.

The amount of expansion that can be attained with the preceding assumptions is limited. As the pressure ratio is decreased, the wake region will converge until an end-point condition of zero width is attained. The pressure ratio at which this condition occurs will depend on the blade spacing, the blade-exit angle, and the thickness of the blade at the trailing edge.

Method 5: Evaluation of flow conditions downstream of row of blades by method of characteristics. - The flow conditions in the exit region of the blades for an assumed Prandtl-Meyer type of expansion with no separation of the flow from the suction-surface wall can be calculated by the method of characteristics (reference 3, pp. 210-232). The flow pattern obtained with this method for the blading configuration used in the experimental program is shown in figure 9. A static-to-total pressure ratio p_4/p'_1 of 0.40 was assigned, as in the evaluation of method 4. It was assumed that no mixing occurred between the main flow issuing from the channel and the stagnant wake regions. The final static pressure p_4 was assumed to exist throughout the wake region up to the trailing edge of the blade, so that separation of the flow from the pressure surface at the trailing edge takes place when the flow from the pressure surface around the trailing edge has turned through the Prandtl-Meyer angle corresponding to the downstream static pressure. Although the flow is initially deflected in the axial direction through the Prandtl-Meyer angle of 4.15°

in region 5 (fig. 9 and table I), subsequent reflections of the expansion waves on the boundary of the jet reverse the direction of deflection progressively so that in region 25 the deflection angle is 4.15° in the tangential direction (or -4.15°, table I). Along the suction surface the expansion waves from the trailing-edge radius are reflected as further expansions so that in region 21 the effective Prandtl-Meyer angle is 8.30°. In order to obtain the downstream static pressure in region 29, a compression wave of 2.15° is necessary at the point of separation from the suction surface. Downstream of the blades the flow pattern becomes repetitive and the general deflection is in the tangential direction. As the exhaust pressure is decreased, the wake region will become continually thinner until the streamlines from adjacent channels cross. At this point, the solution to the problem with the present assumptions is indeterminate.

Method 6: Evaluation of expansion by conservation-of-momentum principle (impulse law) and measured static pressures. - Stodola (reference 4, p. 142) suggests that the deflection of the jet can be analytically determined by application of the conservation-of-momentum principle to the mass of fluid in the region ABCDEFGA, between stations 2 and 4 (fig. 10). The forces acting on the mass of fluid can be conveniently resolved into components parallel and normal to the direction corresponding to the blade angle θ, which is equal to β_2. The pressure force at station 2 P_2 acts in the direction of the velocity at this station and is composed of two parts; $\overline{p_2}A_2$, the average pressure multiplied by the area at station 2, plus $\overline{p_t}A_t$, the pressure force over the trailing-edge area of blade. Acting in the opposite direction are the frictional drag on the suction surface $K_s = \overline{\tau_s} A_s$ and the component of the pressure force at station 4, $P_{a,4}$. Equating these forces to the change in momentum parallel to the suction surface from station 2 to station 4 gives

$$\left.\begin{aligned} m(W_{a,4} - W_2) &= \overline{p_2}A_2 + \overline{p_t}A_t - \overline{\tau_s}A_s - \overline{p_{a,4}}A_{x,4} \\ &= P_2 - K_s - P_{a,4} \end{aligned}\right\} \quad (14a)$$

The components of force and velocity normal to the suction surface of the blade are obtained in a similar manner.

$$\left.\begin{aligned} mW_{n,4} &= \overline{p_s}A_s - \overline{p_{n,4}}A_{x,4} \\ mW_{n,4} &= P_{n,s} - P_{n,4} \end{aligned}\right\} \qquad (14b)$$

The pressure and frictional forces acting on the jet boundary CD will be equal and opposite to those acting on EF.

Critical conditions of flow can be assumed to exist uniformly over the throat section (station 2) if the over-all pressure ratio across the blade row is equal to or less than the critical pressure ratio. The mass flow can be most easily computed at this station.

Only a rough approximation of the frictional drag on the area A_s is necessary for this analysis because the effect of this force on the angle of jet deflection is nearly negligible compared with the pressure forces. The boundary layer is therefore assumed to be turbulent all the way from the leading edge of the blade, and the shearing stress can be calculated from the following equation (reference 6, p. 203):

$$\overline{\tau_s} = \left[\frac{0.059}{(Re_{l,s})^{1/5}}\right]\left[\frac{\overline{\rho_s}\,(\overline{W_s})^2}{2}\right] \qquad (15)$$

where

$$Re_{l,s} = \frac{lW_{av}\rho_{av}}{\mu_{av}}$$

The average values $\overline{\rho_s}$, $\overline{W_s}$, W_{av}, ρ_{av}, and T_{av} for computing μ_{av} can be calculated with sufficient accuracy from the isentropic-flow equations and the static-pressure distribution on the suction surface, which can be determined either experimentally or analytically. (For example, see reference 7.)

The pressure distribution over the areas A_s and $A_{x,4}$ must be experimentally determined. Equation (14b) is then solved for the velocity components $W_{a,4}$ and $W_{n,4}$. The jet-deflection angle is

$$\delta = \tan^{-1}\frac{W_{n,4}}{W_{a,4}} \qquad (16)$$

EXPERIMENTAL APPARATUS AND PROCEDURE

Blade Design

The blade-profile design used in the experimental investigation (fig. 11) is the mean-section profile of a blade for an experimental turbine with 40-percent reaction. The suction surface of the blade from A to B was chosen to be the involute of a circle; from B to C the contour is faired to the straight-line section from C at station 2 to D at the trailing edge. The channel between blades was designed on the basis of one-dimensional-flow theory in such a manner that the mean velocity would continually increase through the channel to the throat section at the exit (station 2). The solidity for this design was 2.2 when based on the axial width and when based on the blade chord was 2.3. This relatively conservative design with a high amount of reaction, gradually increasing radii of curvature of the suction surface, and high solidity was chosen to minimize the possibility of separation of the flow from the blade in the channel and to insure practically constant flow conditions over the width of the throat section for pressure ratios equal to or less than the critical pressure ratio.

Two sizes of blades were used in the investigation. The pressure-distribution surveys were carried out on blades having cross-sectional dimensions three times those given in figure 11. Schlieren photographs were taken of the flow past both the large and small blades. The smaller blades were used in order to increase the number of blades in the cascade for a fixed weight flow so that the flow pattern in the exit region would be uniform and could be observed several chord lengths downstream. In both cases the blade height was 2 inches and the blade profile was constant over the blade height.

Inspection indicated that the maximum deviation of the actual contours from the design was less than 0.003 inch for the 0.60-inch blades and 0.005 inch for the 1.80-inch blades. The maximum deviation of the angle of the trailing edges from the design angle was 0.50° for the 0.60-inch blades and 0.25° for the 1.80-inch blades.

Experimental Equipment

In order to determine experimentally the flow conditions at the exit of the blade row, three cascade configurations of the

rotor-blade design were fabricated. The first was used for making pressure measurements and wake surveys and the other two were used to obtain schlieren photographs of the flow through the blades and downstream of the cascade.

Pressure-survey cascade. - In order to determine the pressure distribution on the blade contour and in the region downstream of the blades, a cascade of six blades having an axial width of 1.80 inches was mounted between horizontal steel plates. The end blocks of the cascade had the same contours as the suction and pressure blade surfaces (fig. 12) so that the cascade included seven equal passages. The static-pressure distribution on the blade surface was obtained for the center passage of the cascade from taps on the surfaces of the center two blades. The location of the pressure taps on the blade contours is shown in figure 11. The 10 taps on the pressure surface and 11 taps on the suction surface upstream of the throat section (station 2) were used to show that the velocity in the channel approached sonic speed at the throat section, and to obtain average values of velocity and density over the suction surface in order to calculate the Reynolds number $Re_{l,s}$. At all pressure ratios smaller than the critical value, the flow conditions through the channel to the throat section remained unchanged. The taps on the straight portion of the suction surface from C to D were spaced approximately 1/16 inch apart. These taps were installed by inlaying 0.015-inch-diameter stainless-steel tubes in a hollowed-out portion of the blade. The area was then filled in with soft solder and shaped to the original contour. The taps were slightly staggered but all were within 0.150 inch of the mean blade height.

Two taps near the center of the upper plate and thirteen taps on the lower plate 0.39 inch upstream of the blade row were used in obtaining the inlet static-pressure distribution to insure that uniform entrance velocities were obtained over the width of the cascade. On the lower plate, downstream of the cascade, 25 static-pressure taps were placed to determine the pressure distribution in this region. The location of all these static-pressure taps is shown in figure 12.

An adjustable wake-survey probe holder was mounted on the upper plate and could be moved along a line parallel to the cascade and 0.45 inch downstream of the blade trailing edges. Probes mounted in this device could be adjusted within 0.010 inch of any desired point in the area to be surveyed and the angle of the probe could be adjusted within 1/4°.

Six-blade optical-survey cascade. - Schlieren photographs of the flow through the cascade of six blades were obtained with a configuration in which the upper and lower plates were made of glass. The blades were pinned to four steel bars about 0.10 inch square in cross section, which were inlaid in slots ground in the glass plates. The assembly of blades, bars, and end blocks was cemented to the glass plates. Five lines evenly spaced 0.08 inch apart around the periphery of one blade were scribed in the spanwise direction. When the flow past these lines was supersonic, the disturbances originated by the lines could be seen in the schlieren photographs and the Mach angle could be measured.

Eighteen-blade optical-survey cascade. - A photograph of the optical-survey configuration similar to the six-blade cascade but having eighteen blades of 0.60-inch axial width is shown in figure 13. Here the blades were fastened to two bars by a pinned tongue-and-groove joint and the bars were laid in slots ground in glass plates. The metal strips on the front edge of the glass plates formed one side of the boundary-layer removal slot (fig. 14) and had pressure taps to obtain the static-pressure distribution over the width of the channel $1\frac{1}{8}$ inches upstream of the blade row. Twelve of the pressure taps on the upper bar and twelve taps on the lower bar were used in obtaining the static-pressure distribution at the entrance over the width of the cascade. The adjustable sheet-metal walls that can be seen in figure 13 extending downstream from the end blocks proved to be impracticable and were removed.

Installation of experimental equipment. - Air from the high-pressure air-supply system of the laboratory was progressively passed through a steam-supplied heat exchanger, a thin-plate orifice for determining the weight flow, and a surge tank 42 inches in diameter and 72 inches in length to insure uniform conditions at the entrance to the test section. The surge tank contained a diaphragm of fine-mesh screens and a bank of flow-straightening tubes for equalizing the velocity distribution over the area of the tank. The test section was mounted directly on the downstream end plate of the surge tank (fig. 14). Air from this test section was exhausted to the low-pressure exhaust system of the laboratory. Two large, horizontal wooden nozzle blocks guided the air from the inside of the surge tank into the test section. The inlet angle was held constant at the design value for all the investigations. Provision was made for drawing off the boundary-layer air from the horizontal walls $1\frac{3}{8}$ inches upstream of the cascade of six blades

used for obtaining the pressure surveys. The boundary-layer ducts extended over the width of the cascade and were divided into four equal sections each having an individual valve for metering the flow. The air from these boundary-layer ducts was exhausted to the low-pressure system of the laboratory.

Optical equipment. - The schlieren optical system is diagrammatically shown in figure 15. A mercury-arc light source was used and a four-microsecond flash was made for each exposure. The two concave aluminized mirrors are 6 inches in diameter and have a focal length of 96 inches. The complex optical system was made necessary by space limitations.

Cascade Calibration

In order to determine the degree to which ideal two-dimensional flow was obtained in the cascade, a detailed survey of the total-pressure distribution in the wake region was made. This survey was made at an over-all static-to-total pressure ratio of 0.60 so that the velocities in the region downstream of the cascade would be subsonic, because it was found that at supercritical pressure ratios the insertion of a probe into the flow caused major disturbances in the static-pressure distribution on the wall below the probe. It was assumed that departures from two-dimensional flow would not be appreciably different at lower pressure ratios. Contours of constant total-pressure loss $(p'_1 - p'_4)/p'_1$ are shown in figure 16 for the lower half of the flow area behind two blades. The location of the points A and B are shown along the line of survey in figure 12. Although there is an area at a blade height from about 0.20 to 0.50 inch in which the total pressure is higher than at the mean blade height (probably caused by secondary flow in the region where the blade meets the wall), the contours are very nearly vertical over the greater part of the blade height. In analyzing the results of the pressure surveys and schlieren photographs of the flow through the cascade configurations using 1.80-inch blades, the departure from two-dimensional flow was therefore neglected. The end-wall effects on the flow through the 0.60-inch blades probably had an even smaller effect on the results because of the greater ratio of length to axial width for these blades.

In addition to the preceding analysis, a survey was made of the flow conditions through the channel with no blades in the cascade. This survey indicated that the flow at the entrance to the blades was parallel to the inlet nozzle blocks within $\pm 2^\circ$.

Experimental Procedure

The inlet temperature in all the experimental investigations was maintained at 600° ±10° R in order to reduce the possibility of condensation and condensation-shock phenomena during the expansion through the blades and in the region downstream of the cascade. Calculations indicated that there was a possibility of condensation only for the lowest pressure ratios.

The inlet total pressure for the cascade of 1.80-inch blades used for the static-pressure surveys was measured in the surge tank and varied from 20 to 43 pounds per square inch absolute; whereas the exhaust pressure was simultaneously varied from 14 to 7 pounds per square inch absolute, depending on the over-all pressure ratio. The general range of pressures used for the investigations of the 0.60-inch blades in the optical-survey configuration was somewhat lower in order not to overstress the blade mounting. The static-to-total pressure ratio for both of these investigations was varied from 0.60 to 0.16. For the static-pressure-distribution investigations, surveys were made at 12 different pressure ratios within this range.

Schlieren photographs with the 0.60-inch blades were taken at eight different pressure ratios. The exit static pressure for the optical-survey configuration was taken as the average of four wall taps (group IV) outside the periphery of the glass plate downstream of the blades (fig. 12). For the optical investigations of the 1.80-inch blades in which the air was exhausted into the room, the inlet pressure was varied from 22 to 35 pounds per square inch absolute and the exhaust pressure was assumed to be atmospheric. Schlieren photographs of this blading configuration were taken at three different pressure ratios.

For the schlieren photographs, the knife edge was adjusted in the focal plane until the maximum constrast between light and dark areas was obtained on a ground-glass screen. At each pressure ratio, photographs were taken at two different knife-edge angles for the 1.80-inch blades and at four different angles for the 0.60-inch blades. In addition, a shadowgraph was obtained of the 0.60-inch blades at each pressure ratio.

For this investigation, the Reynolds number Re_l varied from 6.5×10^5 to 1.7×10^6 for the 1.80-inch blades. Thus, for all the studies with the 1.80-inch blades and most of those with the 0.60-inch blades, the Reynolds number was above the critical range from 10^5 to 3×10^5 and was assumed to have a negligible effect on the results.

In order to obtain uniform flow conditions upstream of the cascade, the weight flow removed through the various boundary-layer-control chambers was adjusted until the variation in the static-pressure distribution upstream of the blades was a minimum. For the investigations with the pressure-survey cascade and for the 0.60-inch blades, the maximum variation in the static-pressure distribution was less than 9 percent of the dynamic pressure.

Instrumentation

The inlet total temperature was measured with a thermocouple and was read on a potentiometer to within 1° F. The static pressures at the inlet to the cascade were read on tetrabromoethane manometers. All the other pressures were read on mercury manometers to an accuracy within 0.05 pound per square inch.

Calculation Methods for Static-Pressure-Survey Data

The flow conditions at the exit of the cascade were evaluated by the momentum relations of method 6 with the data obtained from the static-pressure-distribution surveys. A sample calculation of the evaluation is given in appendix B. A separate analysis was carried out for each of the three groups of exit static-pressure taps, I, II, and III.

Isentropic flow from the stagnation conditions in the surge tank to critical conditions at the throat section (station 2) of the blades was assumed. The mass flow was calculated from these assumed conditions at station 2 and an assumed flow coefficient of unity.

The pressure force $P_{n,s}$ was evaluated by integrating a plot of the static-pressure distribution over the area A_s against the projection of the line AGF (fig. 10) on a line parallel to the flow direction at station 2. The pressure $\overline{p_t}$ was read from this curve at the point corresponding to the projection of trailing-edge point F. The boundary-layer shearing stress $\overline{\tau_s}$ was evaluated by equation (15), and average values of density and velocity were evaluated from the experimentally determined static-pressure distribution over the suction surface of the blade, assuming isentropic-flow conditions. The average exit static pressure for each of the three rows of taps was used in each of the three separate analyses.

RESULTS AND DISCUSSION

The results of the experimental evaluation of the deflection angle by the conservation-of-momentum principle of method 6 are compared with the results of the theoretical methods 1, 2, and 3. The analysis of the schlieren photographs is presented and shows the extent to which the assumptions of methods 4 and 5 are justified.

Static-Pressure Surveys

The results of the experimental evaluation of the deflection angle using the static-pressure-survey data and the momentum relations of method 6 are shown in figure 17. The deflection angle is plotted against the isentropic critical-velocity ratio corresponding to the pressure ratio p_4/p'_1 at that point. For all three rows of downstream static-pressure taps, negative deflection angles are obtained for values of $(W_4/W_{cr})_1$ less than about 1.27. Although there is considerable scatter of the data points for these values, the deflection angle tends to become less negative as the flow progresses from group I to III for these low velocity ratios. This effect is probably due to losses in this region, which cause a gradual change in flow angle toward the axial direction. At higher velocity ratios, comparatively large positive deflection angles are obtained and the agreement between points is considerably improved.

The ratio of the actual velocity at pressure group I (determined by method 6) to the critical velocity, and the axial and tangential critical-velocity ratios are plotted against the isentropic critical-velocity ratio at this station in figure 18. The difference between the isentropic and actual velocities varies from about 3 percent of the ideal value at the upper end of the curve to 10 percent at the lower end. This range of velocity difference corresponds to efficiencies of the expansion from 0.94 to 0.83, respectively.

The tangential-velocity ratio $(W_{u,4}/W_{cr})_{ac}$ increases until $(W_4/W_{cr})_1$ is equal to about 1.14 and then remains practically constant at a value of 1.01. The aerodynamic loading of the blade reaches its maximum value at this point and then remains constant, so that no further increase in the tangential-velocity component can be obtained. The pressure distribution over the area A_s for

this condition of maximum loading is shown in figure 19. The continually decreasing pressure from the throat to the trailing edge of the blade indicates continued acceleration of the flow along the surface and therefore it is unlikely that separation of the flow from the surface occurs for the condition of maximum loading.

Even though the over-all pressure ratio across the cascade test section $p_{4,IV}/p'_1$ was varied from 0.22 to 0.18 (the minimum value attainable with the experimental equipment) for the last three points on the curve for pressure-tap group I in figure 17 and on each curve in figure 18, these points are practically superimposed, which indicates that any decrease in the exhaust pressure to give pressure ratios less than 0.22 will not change the flow conditions at pressure-tap group I. This end-point condition occurs at a supercritical exit axial-velocity ratio.

In a turbine having a constant annular area downstream of the blades, the passage would become choked at an axial Mach number of unity and the curves of figures 17 and 18 would end at a value of $(W_4/W_{cr})_i$ of 1.48. In the cascade investigation, however, the exhaust static pressure influenced the flow immediately downstream of the cascade, even when the axial velocity was supersonic, until the end-point condition was attained at a value of $(W_{4,I}/W_{cr})_i$ of 1.56. The condition existing at this point was evaluated from an analysis of the schlieren photographs. A similar condition would probably be obtained in an actual turbine if the annular area downstream of the rotor increased sufficiently to allow supersonic axial-velocity ratios.

The dashed curve in figure 18, originating at the point (1,1), is a plot of the velocity ratio W_4/W_{cr} calculated by method 3, which assumes a constant tangential velocity from station 3. The end point of the curve corresponds to sonic axial velocity. For values of $(W_4/W_{cr})_i$ greater than 1.1, the velocities calculated by method 3 are considerably lower than the experimental values. In order to approximate more closely the experimentally determined points, an additional evaluation of the final flow conditions was made using a combination of methods 1 and 3. It was assumed that the expansion from station 2 to 4 takes place according to the assumptions of method 1 until the tangential critical-velocity ratio $W_{u,4}/W_{cr}$ attains the experimentally determined constant value of 1.01. The corresponding value of $(W_4/W_{cr})_i$ is about 1.14. For higher values of the critical-velocity ratio $(W_4/W_{cr})_i$,

the conditions at station 4 were evaluated by assuming, as in method 3, that the expansion takes place with losses and with a constant tangential velocity. The values of W_4/W_{cr} obtained with the combination of methods 1 and 3 are plotted in figure 18 beginning at the point (1.14, 1.14). The velocity calculated by this method closely checks the experimental values obtained from method 6 after the tangential-velocity ratio reaches a constant value. Sonic axial velocity is obtained for $(W_4/W_{cr})_i$ equal to 1.45 for this experimental method of evaluation.

A comparison of the flow-deflection angles determined by methods 1, 2, 3, the combination of methods 1 and 3, and the experimental results of method 6 at pressure-tap group I is presented in figure 20. The curve for method 1 deviates from the experimentally determined points after the loading of the rear portion of the blade has reached its maximum value. At the point of sonic axial velocity, the deflection angle calculated by method 1 is only 2°, whereas the measured value is approximately 11°. As expected, method 2 gives deflection angles far in excess of the actual value when the flow areas $A_{x,3}$ and $A_{x,4}$ are equal. Of these three original methods, method 3 gives the best correlation with the experimental data. However, although the data points for the negative deflection angles are rather scattered, deflection angles of the order of -6° were obtained for $(W_{4,I}/W_{cr})_i$ as high as 1.15.

The curve of the deflection angles calculated by the combination of methods 1 and 3 gives the closest correlation with the experimentally determined values of the deflection angle. This method could be used to determine theoretically the angle of flow deflection for the general case if the point at which the aerodynamic loading of the rear portion of the blade reaches its maximum value could be predicted. An analysis of the schlieren photographs of the flow shows the complex phenomena that occur at supercritical pressure ratios and indicates the difficulties in predicting this point of maximum loading.

Schlieren Photographs

Three of the schlieren photographs of the flow through the 1.80-inch blades are presented in figure 21. The photographs were taken at three different pressure ratios with the schlieren knife edge parallel to the inlet-flow direction. Because the blades turn the incoming air through an angle of about 90°, for all

practical purposes the knife edge is perpendicular to the flow direction downstream of the cascade. Areas having greater light intensity than the region of negligible density gradient at the top of each photograph can be shown to have positive density gradient in the direction from left to right, perpendicular to the knife edge.

A comparison of the three photographs of figure 21 shows the progressive change in the flow pattern that takes place with decreasing values of the pressure ratio p_4/p'_1. Figure 21(a) shows that, at static-to-total pressure ratios considerably greater than that required to give critical flow at the throat section, the static pressure immediately upstream of the throat is slightly lower than the exhaust pressure and a region of compression originates on the pressure surface of the blade near the trailing edge. The measured static-pressure distribution on the pressure surface for the same over-all pressure ratio confirms this result.

Figure 21(b) shows that as the pressure ratio is decreased to 0.52, slightly less than the critical pressure ratio, the region of compression becomes a weak shock wave that is nearly normal to the flow. Further expansion takes place downstream of this shock as evidenced by the dark region followed by a second compression shock originating from the suction surface at the trailing edge.

As the pressure ratio is further decreased to 0.42 (the minimum obtainable with this blade configuration exhausting to the atmosphere), corresponding to a value of $(W_4/W_{cr})_1$ of 1.15, the two shock waves tend to become stronger and more oblique until the complex flow pattern shown in figure 21(c) is obtained. The deflection angle is still negative, as indicated in figure 17.

An enlargement of a photograph of the flow for a pressure ratio of 0.42 at the exit of two of the passages with the schlieren knife edge parallel to the flow in this region is shown in figure 22. With this knife-edge orientation, the oblique shock wave originating from the pressure surface at the trailing edge is light, whereas the one from the suction surface is dark. The fine lines scribed over the blade span on the suction surface of the center blade caused Mach lines that were used to measure the Mach angles.

An evaluation by the method of characteristics of the flow conditions in figure 22 is given in figure 23. The expansion from the pressure surface around the trailing-edge radius takes place as assumed in methods 4 and 5. The flow does not separate, however, from the trailing edge after expanding to a Prandtl-Meyer angle of 3.2° corresponding to the static-to-total pressure ratio of 0.42, but expands through a Prandtl-Meyer angle of about 9° to region 2 before passing through the oblique compression shock C_p. The pressure distribution on the suction surface for this condition is given in figure 24. No separation from the suction surface was assumed to occur until the measured pressure distribution differed from that calculated by the method of characteristics in method 5. The oblique shock C_p originating from the deflection of the flow from the pressure surface after region 2 (fig. 23) is reflected from the region of flow separation adjacent to region 4 as a series of expansion waves. A region of compression follows and then further expansion occurs around the trailing edge to the oblique shock C_s, which extends across the flow from several channels (fig. 21(c)).

Measurement of the flow angle of the wake regions from photographs similar to that of figure 21 gave reasonably close agreement with the experimental results of method 6. The wake regions are not defined clearly enough in the photographs to make such measurements accurate to more than ±3°.

Photographs of the flow through the cascade of 0.60-inch blades are shown in figure 25. The flow pattern in figure 25(a) is comparable with that in figure 21(c), which was taken at very nearly the same pressure ratio. The shock waves discussed in the analysis of figure 23 extend several chord lengths downstream of the blades. The shock wave C_s originating from the deflection of the flow separated from the suction surface downstream of the trailing edge is stronger than the one originating at the point of separation of the flow from the suction surface.

A shadowgraph taken at a pressure ratio of 0.39 is shown in figure 25(b). The analysis by method 6 indicates that at this pressure ratio the tangential-velocity component reaches its maximum value. The angle of the oblique shock C_p is decreased so that it no longer affects the pressure distribution on the suction surface. Simultaneously, the point of flow separation from the suction surface has moved so close to the trailing edge that it is evident that the rear portion of the blade has practically reached the maximum-loading condition.

As the pressure ratio was lowered from the point at which the photograph of figure 25(b) was taken, the oblique shocks C_p crossing the passages between blade trailing edges turn progressively farther downstream (fig. 25(c)). The flow at the exit of the upper blades in this photograph has attained the supersonic end-point condition discussed in the analysis of method 6. A further reduction in the downstream pressure does not change the conditions at the exit of the upper blades but only extends the region of this maximum expansion to all the blades in the cascade (fig. 25(d)). The shock waves C_s originating from the suction surface at the trailing edge are relatively strong and extend all the way across the field of the picture; whereas some of the shock waves C_p originating from the pressure surface of the trailing edges of the center blades are dissipated near the top of the photograph.

A quantitative analysis of an enlargement of another schlieren photograph of this end-point condition (fig. 26) was carried out using the method of characteristics. The resulting flow pattern is shown in figure 27 and the flow conditions given in table II. Flow conditions before and after each of the theoretical shock waves at the measured positions were determined by a process of trial-and-error by which the conditions ahead of the shock wave were selected to satisfy the Prandtl-Meyer expansion from the pressure surface of the blade around the trailing edge. In this manner it was possible to calculate theoretical shock waves that agreed with the measured ones from the photograph within the accuracy of such measurements, which was $\pm 2^\circ$. The experimental pressure distribution along the suction surface (fig. 19) agrees well with the theoretical values calculated in this analysis.

The flow is continuously supersonic at the exit, with extremely thin wake regions at this pressure ratio. Any further decrease in the exhaust pressure cannot appreciably change the flow conditions at the exit of the blades. The sets of shock waves C_p and C_s extend almost unchanged a long distance downstream of the blade row. The shock wave C_s is the stronger one and deflects the flow through an angle of about 12° as compared with about 5° for the shock wave C_p. Because the expansion waves are not exactly parallel to the shock waves, the shock waves will eventually be dissipated, which probably explains the thinning out of the shock waves C_p at the top of figure 25(d).

The exit deflection angle δ varies from approximately 7° to 19° from region 8 to 10. The mass-averaged value of the deflection angle along the line of static-pressure-tap group I, calculated from figure 27, was found to be 16.7°, 2° greater than the maximum value of 14.7° determined by method 6.

The foregoing results show that, contrary to the assumption of method 4, the flow does not separate from the suction surface in the manner shown in figure 7. Deflection of the flow in the axial direction is not attained until the exit static pressure is considerably below that required to give critical-flow conditions at station 2. Although method 5 gives a closer approximation to actual conditions, it does not give the point of maximum loading of the rear portion of the blade without additional information about the flow conditions in this region.

SUMMARY OF RESULTS

A comparison of the results of five theoretical methods for determining the deflection angle at the exit of a row of blades at supercritical pressure ratios with an experimental method using static-pressure surveys, and also with schlieren photographs, yielded the following results:

1. Experimental results indicated that even at pressure ratios considerably lower than that required to give critical velocity at the throat section, the flow was deflected in the tangential direction as predicted for the incompressible case.

2. As the pressure ratio was continually lowered, the aerodynamic loading of the blade reached a maximum value and then remained constant. After this condition was attained, the expansion downstream of the cascade took place with a constant tangential velocity so that no further increase in the amount of turning across the blade row and no further increase in the loading of the blade was available.

3. None of the five methods for analytically determining the jet-deflection angle gave results that agreed closely with the experimental results. The assumption of nonisentropic expansion with a constant value of tangential-velocity component after the aerodynamic loading of the rear portion of the blade reached its maximum value gave the best agreement between theory and experiment.

4. When the entire field of flow a short distance downstream of the blades became supersonic, an end-point condition for which the axial velocity was supersonic was attained. Any further decrease in the pressure ratio after this condition was attained did not change the flow conditions at the exit of the blades.

5. The deflection of the jet for the blades investigated in the cascade was found to be about 7° in the tangential direction until the blade loading reached its maximum value; the deflection angle then changed as the pressure ratio was further decreased, until a maximum value of about 15° in the axial direction was obtained for the end-point condition.

Lewis Flight Propulsion Laboratory,
National Advisory Committee for Aeronautics,
Cleveland, Ohio.

APPENDIX A

DERIVATION OF RELATION BETWEEN AXIAL- AND TANGENTIAL-VELOCITY COMPONENTS WHEN AXIAL COMPONENT IS EQUAL TO SONIC VELOCITY

From the condition of continuity and the isentropic one-dimensional-flow relations, it is known that the axial-velocity component will be sonic at the point for which the mass flow is a maximum. Because the area in planes perpendicular to the axial direction is constant, the maximum mass flow will be obtained when ρW_x is maximum.

From the isentropic-flow relations,

$$\frac{\rho}{\rho'}\frac{W_x}{W_{cr}} = \left\{1.0 - \frac{\gamma-1}{\gamma+1}\left[\left(\frac{W_x}{W_{cr}}\right)^2 + \left(\frac{W_u}{W_{cr}}\right)^2\right]\right\}^{\frac{1}{\gamma-1}}\left(\frac{W_x}{W_{cr}}\right)$$

By setting the derivative with respect to the axial component equal to zero,

$$\frac{d\left(\frac{\rho}{\rho'}\frac{W_x}{W_{cr}}\right)}{d\left(\frac{W_x}{W_{cr}}\right)} = \left\{1.0 - \frac{\gamma-1}{\gamma+1}\left[\left(\frac{W_x}{W_{cr}}\right)^2 + \left(\frac{W_u}{W_{cr}}\right)^2\right]\right\}^{\frac{1}{\gamma-1}}$$

$$\frac{1}{\gamma-1}\left\{1.0 - \frac{\gamma-1}{\gamma+1}\left[\left(\frac{W_x}{W_{cr}}\right)^2 + \left(\frac{W_u}{W_{cr}}\right)^2\right]\right\}^{\frac{2-\gamma}{\gamma-1}}\left(2\,\frac{\gamma-1}{\gamma+1}\right)\left(\frac{W_x}{W_{cr}}\right)^2 = 0$$

By solving for the axial component,

$$\frac{W_x}{W_{cr}} = \sqrt{1.0 - \frac{\gamma-1}{\gamma+1}\left(\frac{W_u}{W_{cr}}\right)^2} \qquad (4)$$

APPENDIX B

SAMPLE CALCULATION FOR METHOD 6 — EVALUATION OF EXPANSION BY USE OF CONSERVATION-OF-MOMENTUM METHOD (IMPULSE LAW) AND MEASURED VALUES OF STATIC-PRESSURE DISTRIBUTION

The various quantities in equations (14a) and (14b) may be evaluated as follows:

1. Evaluation of P_2 and W_2:

$$P_2 = \overline{p_2} A_2 + \overline{p_t} A_t$$

$$\overline{p_2} = p_{cr} = \left(\frac{2}{\gamma+1}\right)^{\frac{\gamma}{\gamma-1}} p'_1$$

$$= \left(\frac{2}{2.40}\right)^{\frac{1.40}{0.40}} (144)(34.88) \text{ lb/sq ft}$$

$$A_2 = 0.00525 \text{ sq ft}$$

$$\overline{p_2} A_2 = 13.93 \text{ lb}$$

From figure 19, which is a plot of the static-pressure distribution over the area A_s for the point of maximum loading, the pressure $\overline{p_t}$ is

$$\overline{p_t} = 3.20 \text{ lb/sq in.}$$

$$\overline{p_t} A_t = (3.20)(144)(0.00125)$$

$$= 0.58 \text{ lb}$$

$$P_2 = 13.93 + 0.58$$

$$= 14.51 \text{ lb}$$

$$W_2 = W_{cr} = \sqrt{\frac{2\gamma}{\gamma+1} gRT'_1}$$

$$= \sqrt{\frac{2(1.40)}{2.40} (32.17)(53.34)(607)}$$

$$= 1101.9 \text{ ft/sec}$$

2. Evaluation of K_s:

$$K_s = \overline{\tau_s} A_s$$

$$\overline{\tau_s} = \left[\frac{0.059}{(Re_{l,s})^{1/5}}\right]\left[\frac{\overline{\rho_s} (\overline{W_s})^2}{2}\right] \qquad (15)$$

where

$$Re_{l,s} = \frac{l W_{av} \rho_{av}}{\mu_{av}}$$

$$= \frac{(0.181)(937)(0.00350)}{3.81 \times 10^{-7}}$$

$$= 1.56 \times 10^6$$

$$\overline{\tau_s} = \frac{0.059}{(1.56 \times 10^6)^{1/5}} \frac{(0.00207)(1460)^2}{2}$$

$$= 7.5 \text{ lb/sq ft}$$

$$K_s = (7.5)(0.01025) = 0.08 \text{ lb}$$

3. Evaluation of $P_{a,4}$ and $P_{n,4}$:

$$P_{a,4} = \overline{p_{a,4}} A_{x,4}$$

$$\overline{p_{a,4}} = \overline{p_4} \sin \beta_2$$

$$P_{a,4} = (5.581)(144)(0.5616)(0.01158)$$

$$= 5.23 \text{ lb}$$

$$P_{n,4} = \overline{p_{n,4}} A_{x,4}$$

$$\overline{p_{n,4}} = \overline{p_4} \cos \beta$$

$$P_{n,4} = (5.581)(144)(0.8274)(0.01158)$$

$$= 7.70 \text{ lb}$$

4. Evaluation of $P_{n,s}$:

$$P_{n,s} = \overline{p_s} A_s$$

$$= 2.0 \text{ (area under plot of static pressure against distance along area, } A_s, \text{ fig. 19)}$$

$$= 2.0 (7.63)$$

$$P_{n,s} = 15.26 \text{ lb}$$

5. Evaluation of m:

$$m = \rho_{cr} W_{cr} A_2$$

$$\rho_{cr} = \left(\frac{2}{\gamma+1}\right)^{1/\gamma} \rho'_1$$

$$m = (0.6339)(0.004822)(1101.8)(0.00525)$$

$$= 0.01769 \text{ slug/sec}$$

6. Evaluation of $W_{a,4}$, $W_{n,4}$, and δ:

$$m(W_{a,4} - W_2) = P_2 - K_s - P_{a,4} \qquad (14a)$$

$$mW_{n,4} = P_{n,s} - P_{n,4} \tag{14b}$$

$$(0.01769)(W_{a,4} - 1101.9) = 14.51 - 0.08 - 5.23 \tag{14a}$$

$$W_{a,4} = 1622 \text{ ft/sec}$$

$$(0.01769)\, W_{n,4} = 15.26 - 7.70 \tag{14b}$$

$$W_{n,4} = 427 \text{ ft/sec}$$

$$\delta = \tan^{-1} \frac{W_{n,4}}{W_{a,4}}$$

$$= \tan^{-1} \frac{427}{1622}$$

$$= 14.75^{\circ}$$

7. Evaluation of $\left(\frac{W_{4,I}}{W_{cr}}\right)_i$:

$$\left(\frac{W_{4,I}}{W_{cr}}\right)_i = \sqrt{\frac{\gamma+1}{\gamma-1}\left[1 - \left(\frac{\overline{p_{4,I}}}{p'_1}\right)^{\frac{\gamma-1}{\gamma}}\right]}$$

$$\frac{\overline{p_{4,I}}}{p'_1} = 0.160$$

$$\left(\frac{W_{4,I}}{W_{cr}}\right)_i = 1.564$$

REFERENCES

1. Emmert, H. D.: Current Design Practices for Gas Turbine Power Elements. Paper No. 48-A-69, presented before Ann. Meeting A.S.M.E. (New York), Nov. 28-Dec. 3, 1948.

2. Anon.: Third Report of the Steam-Nozzles Research Committee. Proc. Inst. Mech. Eng. (London), vol. I, Jan.-May 1924, pp. 455-501; discussion, pp. 502-525.

3. Liepmann, Hans Wolfgang, and Puckett, Allen E.: Introduction to Aerodynamics of a Compressible Fluid. John Wiley & Sons, Inc., 1947, pp. 23-37, 189-232.

4. Stodola, A.: Steam and Gas Turbines. Vol. I. McGraw-Hill Book Co., Inc., 1927, pp. 136-146.

5. Kochendorfer, Fred D., and Nettles, J. Cary: An Analytical Method of Estimating Turbine Performance. NACA RM E8I16, 1948.

6. Rouse, Hunter: Fluid Mechanics for Hydraulic Engineers. McGraw-Hill Book Co., Inc., 1938, pp. 203-204.

7. Huppert, M. C., and MacGregor, Charles: Comparison between Predicted and Observed Performance of Gas-Turbine Stator Blade Designed for Free-Vortex Flow. NACA TN 1810, 1949.

TABLE I - FLOW CONDITIONS FOR ANALYSIS BY METHOD OF CHARACTERISTICS AS SHOWN IN FIGURE 9

Region	Prandtl-Meyer angle (deg)	Flow-deflection angle, δ (deg)	Region	Prandtl-Meyer angle (deg)	Flow-deflection angle, δ (deg)
1	0	0	37	5.15	1.15
2	1.00	1.00	38	4.15	.15
3	2.00	2.00	39	4.15	-1.85
4	3.00	3.00	40	3.00	-3.00
5	4.15	4.15	41	6.15	.15
6	2.00	0	42	5.15	-.85
7	3.00	1.00	43	4.15	-1.85
8	4.00	2.00	44	4.15	-4.15
9	5.15	3.15	45	7.30	-1.00
10	4.15	2.15	46	6.30	-2.00
11	4.00	0	47	5.30	-3.00
12	5.00	1.00	48	4.15	-4.15
13	6.15	2.15	49	4.15	2.15
14	5.15	1.15	50	3.15	1.15
15	4.15	.15	51	2.15	.15
16	6.00	0	52	1.00	-1.00
17	7.15	1.15	53	4.15	2.15
18	6.15	.15	54	4.15	.15
19	5.15	-.85	55	3.15	-.85
20	4.15	-1.85	56	2.00	-2.00
21	8.30	0	57	5.15	1.15
22	7.30	-1.00	58	4.15	.15
23	6.30	-2.00	59	4.15	-1.85
24	5.30	-3.00	60	3.00	-3.00
25	4.15	-4.15	61	6.15	.15
26	6.30	0	62	5.15	-.85
27	5.30	-1.00	63	4.15	-1.85
28	4.30	-2.00	64	4.15	-4.15
29	4.15	2.15	65	7.30	-1.00
30	3.15	1.15	66	6.30	-2.00
31	2.15	.15	67	5.30	-3.00
32	1.00	-1.00	68	4.15	-4.15
33	4.15	2.15	69	4.15	2.15
34	4.15	.15	70	3.15	1.15
35	3.15	-.85	71	2.15	.15
36	2.00	-2.00	72	1.00	-1.00

TABLE II - FLOW CONDITIONS FOR ANALYSIS OF FIGURE 22 BY METHOD OF CHARACTERISTICS AS SHOWN IN FIGURE 23

Region	Prandtl-Meyer angle (deg)	Flow-deflection angle, δ (deg)
1	0	0
2	9.0	9.0
3	9.0	1.0
4	8.0	10.0
5	2.7	-1.1
6	1.0	1.0
7	5.0	5.0
8	3.0	7.0
9	9.0	1.0
10	5.0	4.3

TABLE III - FLOW CONDITIONS FOR ANALYSIS OF FIGURE 26 BY METHOD OF CHARACTERISTICS AS SHOWN IN FIGURE 27

Region	Prandtl-Meyer angle (deg)	Flow-deflection angle, δ (deg)
1	0	0
2	29.0	29.0
3	21.7	22.0
4	18.4	18.8
5	25.0	1.0
6	28.0	6.0
7	19.0	14.6
8	30.6	6.8
9	23.0	24.4
10	17.5	19.1
11	32.0	20.0
12	24.5	12.8
13	26.0	14.3
14	29.0	17.2
15	23.5	11.9
16	25.0	13.4

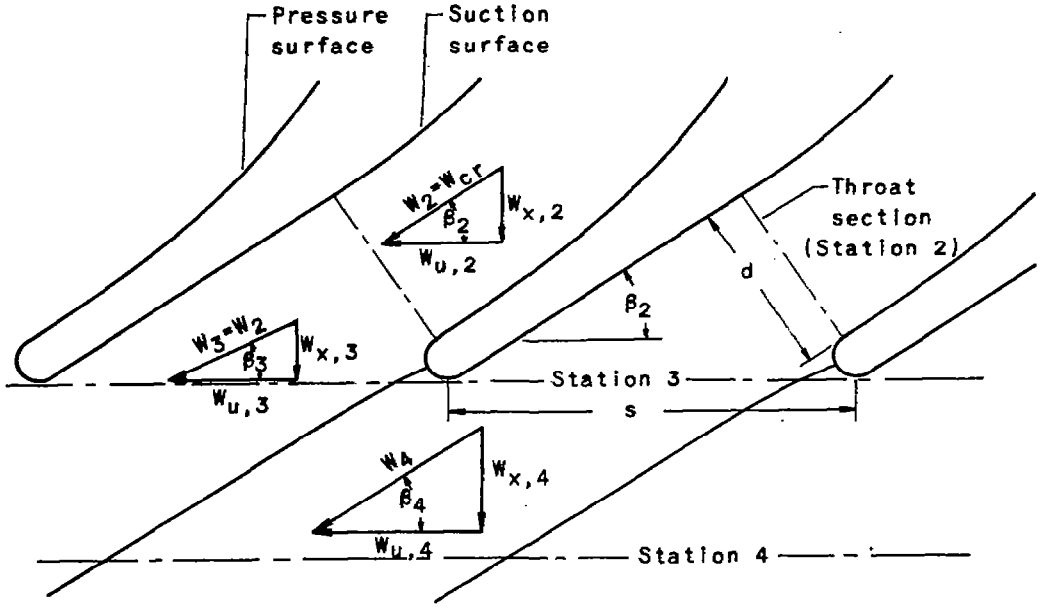

Figure 1. – Diagram of flow conditions at exit of cascade of turbine rotor blades at supercritical pressure ratios for Method I assuming isentropic expansion with constant flow area in planes perpendicular to axial direction.

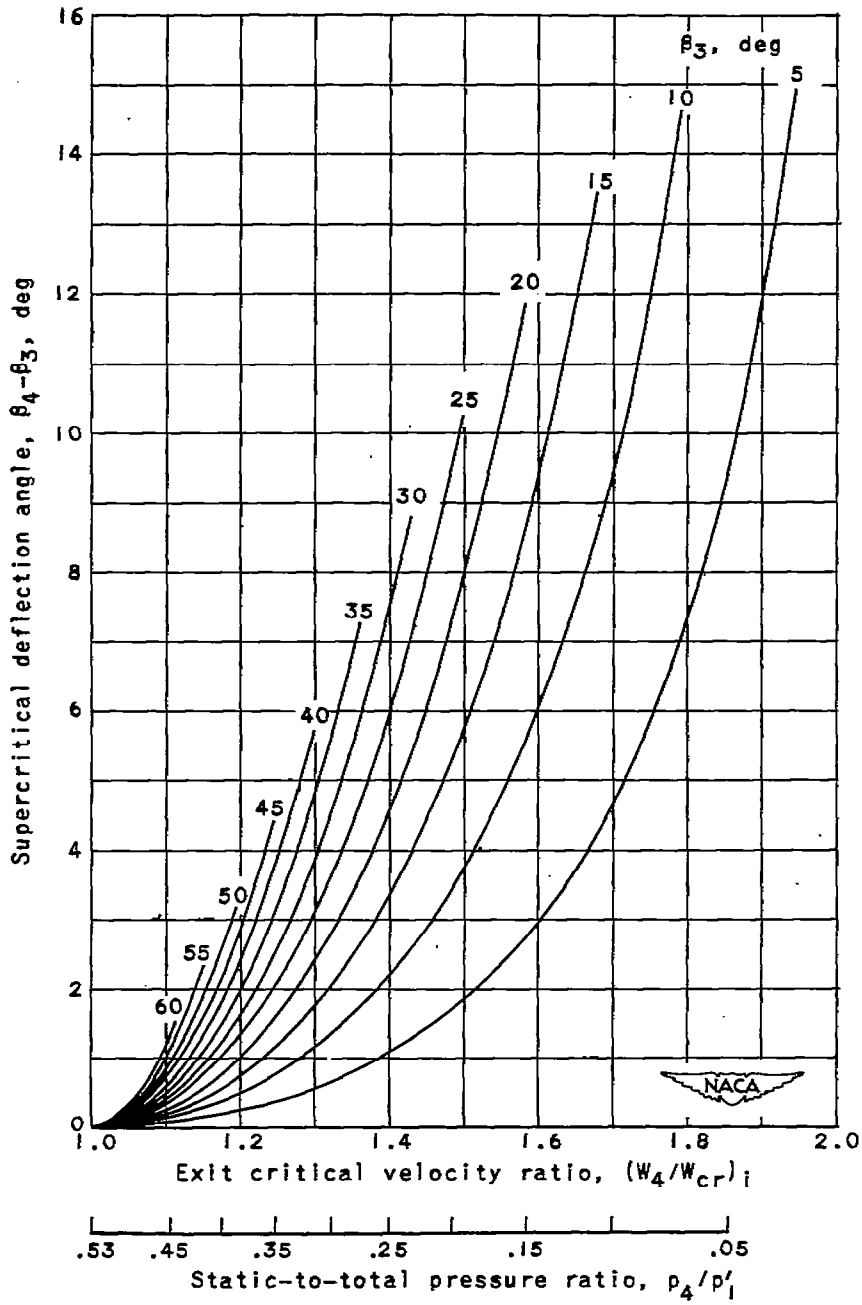

Figure 2. - Variation of supercritical portion of deflection angle $\beta_4-\beta_3$ with exit critical velocity ratio for Method I assuming isentropic expansion with constant flow area in planes perpendicular to axial direction. $\gamma = 1.4$.

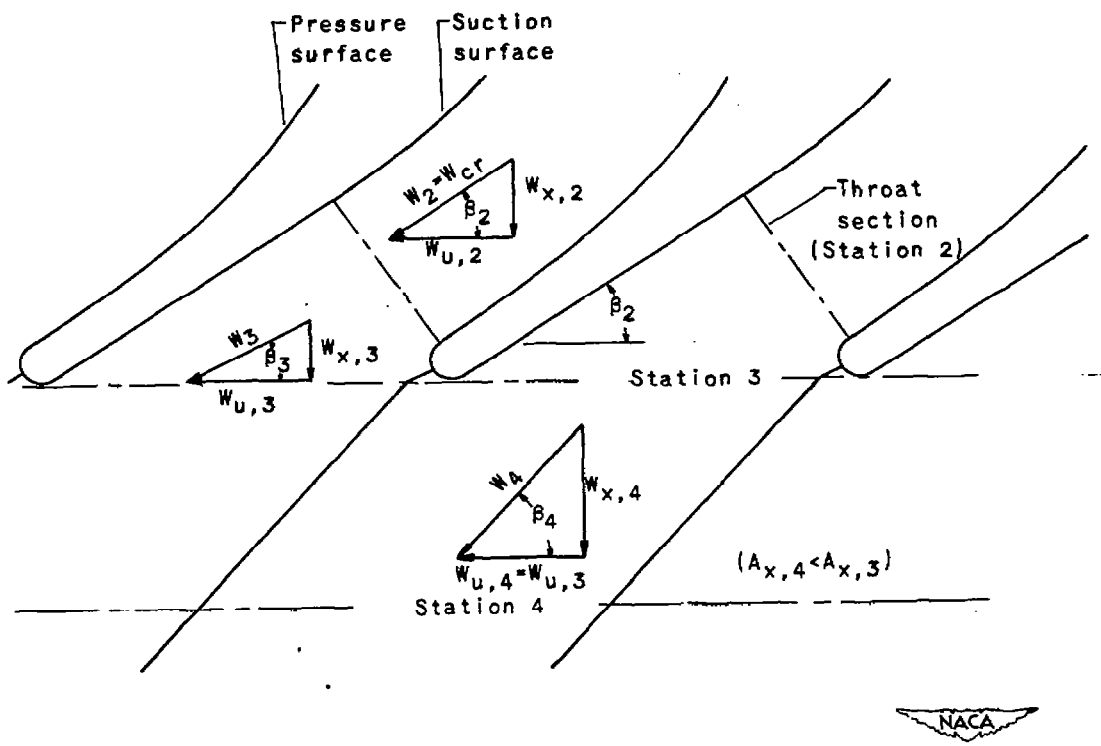

Figure 3. - Diagram of flow conditions at exit of cascade of turbine rotor blades at supercritical pressure ratios for Method 2 assuming isentropic expansion with constant value of tangential component of velocity.

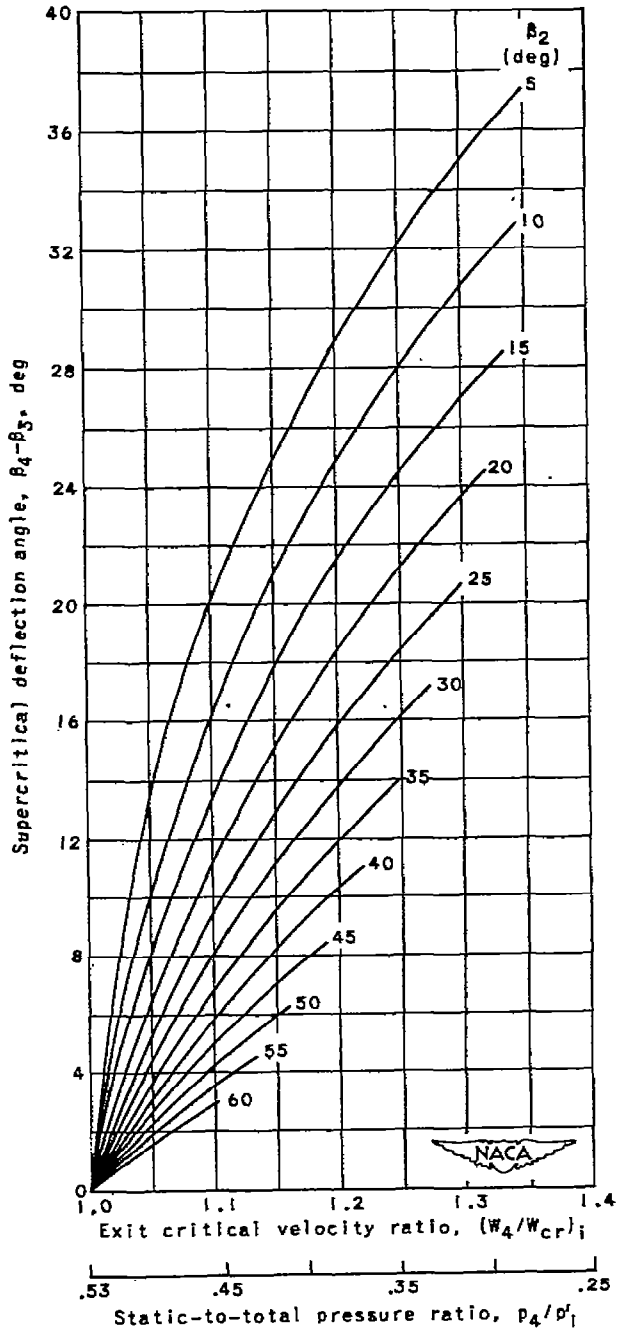

Figure 4. - Variation of supercritical portion of deflection angle $\beta_4-\beta_3$ with exit critical velocity ratio for Method 2 assuming isentropic expansion with constant value of tangential component of velocity. $\gamma = 1.4$.

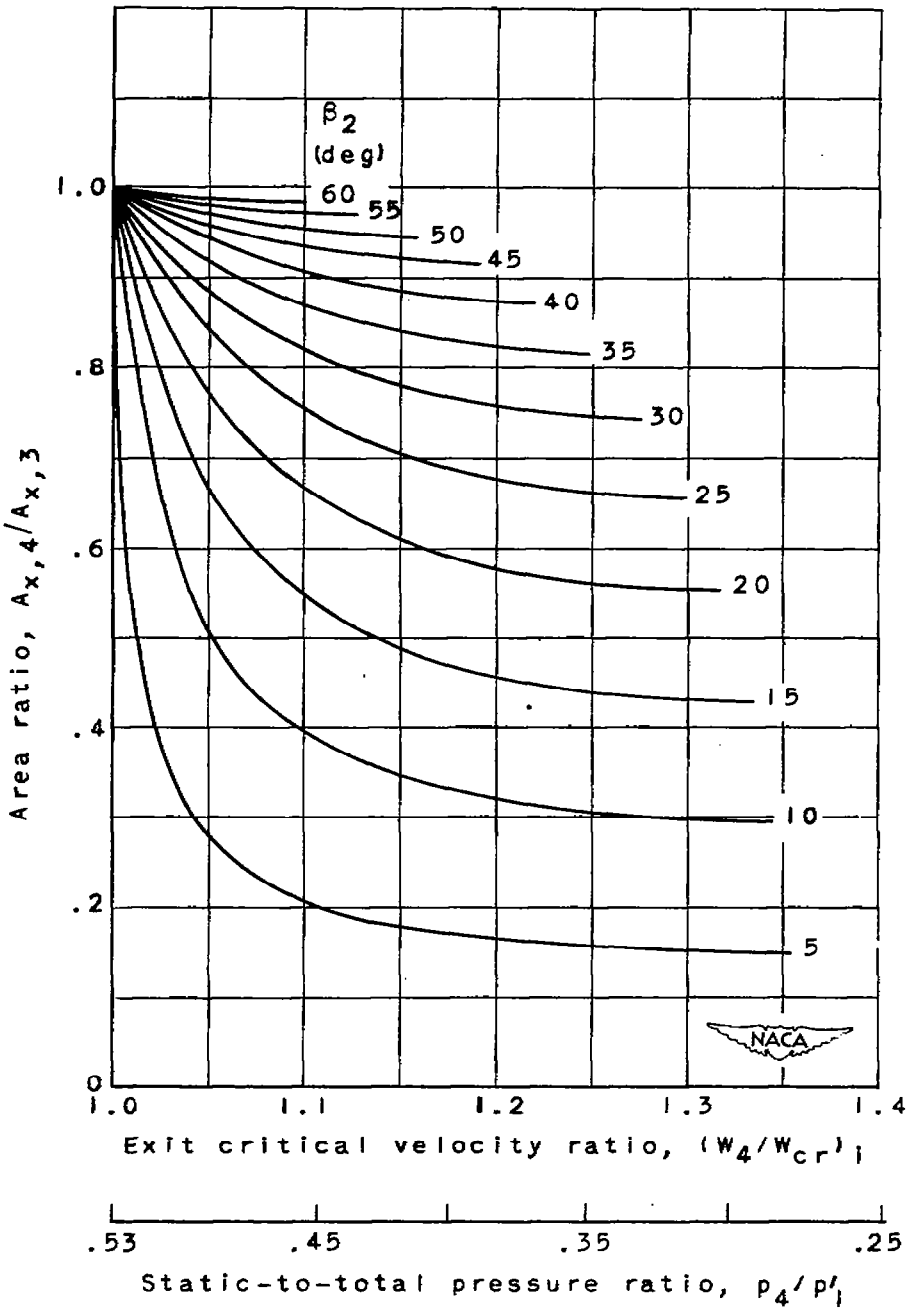

Figure 5. – Area ratio $A_{x,4}/A_{x,3}$ at exit of cascade of turbine rotor blades for Method 2 assuming isentropic expansion with constant value of tangential component of velocity. γ = 1.4.

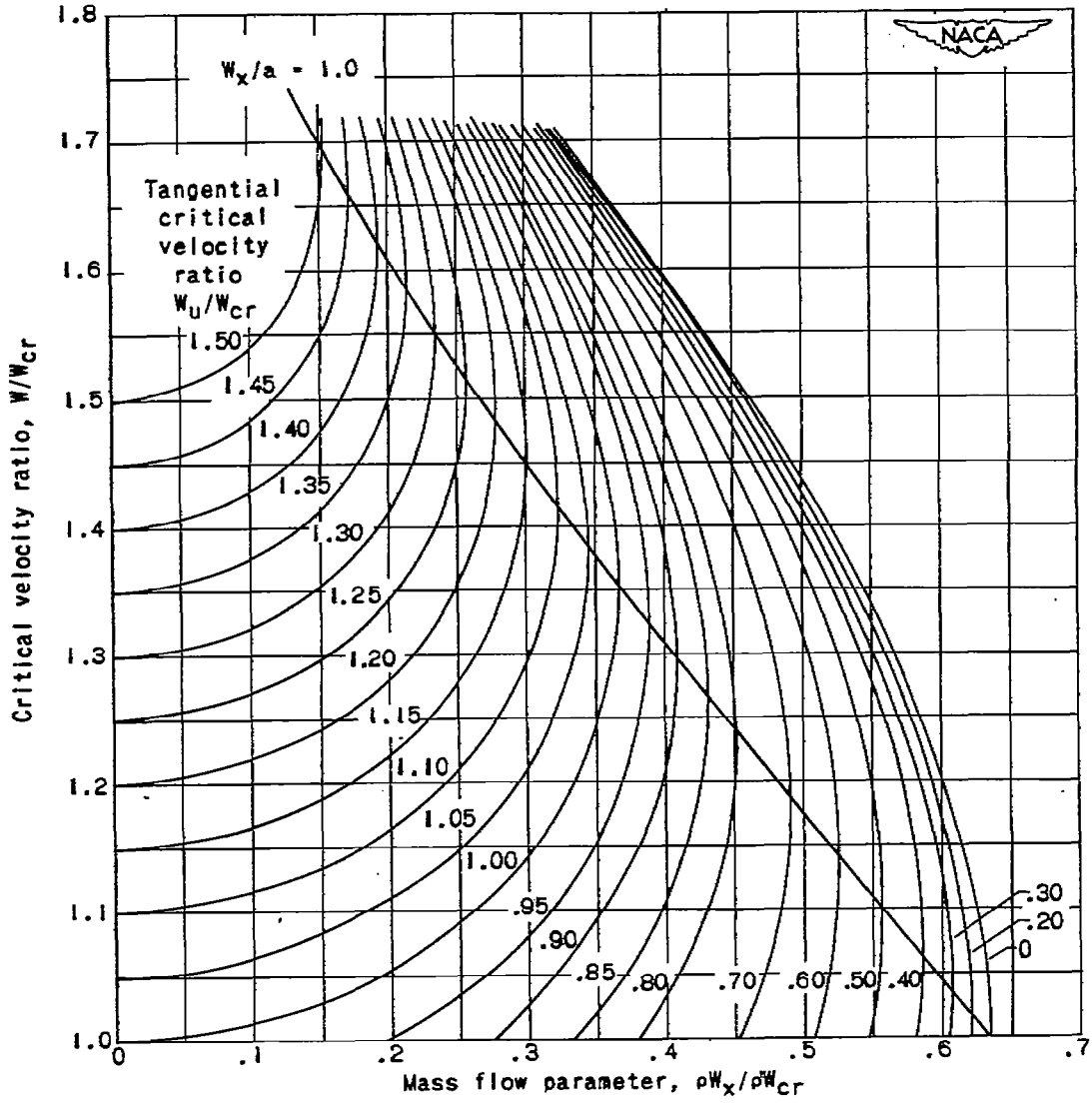

Figure 6. - Graph for determining flow conditions at station 4 for Method 3 assuming nonisentropic expansion with constant value of tangential component of velocity and constant flow area in planes perpendicular to axial direction. $\gamma = 1.4$.

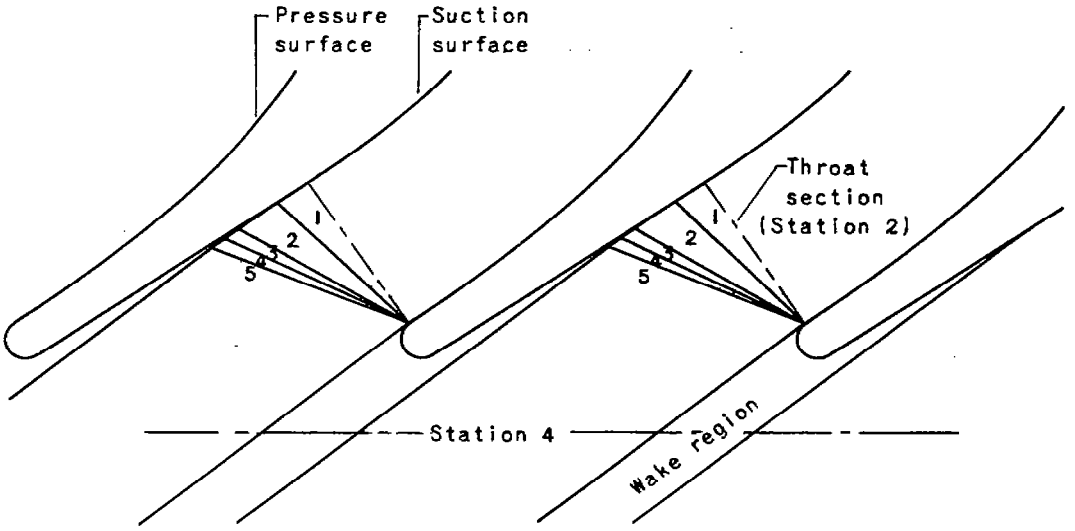

Region	Prandtl-Meyer angle (deg)	Pressure ratio p/p'_1	Critical velocity ratio W/W_{cr}
1	0	0.5283	1.0000
2	1.00	.4791	1.0667
3	2.00	.4498	1.1066
4	3.00	.4249	1.1409
5	4.15	.4000	1.1757

Figure 7. - Diagram of flow conditions at exit of cascade of turbine rotor blades at static-to-total pressure ratio of 0.400 for Method 4 assuming isentropic expansion of flow with deflection toward axial direction according to Prandtl-Meyer theory of flow around a corner.

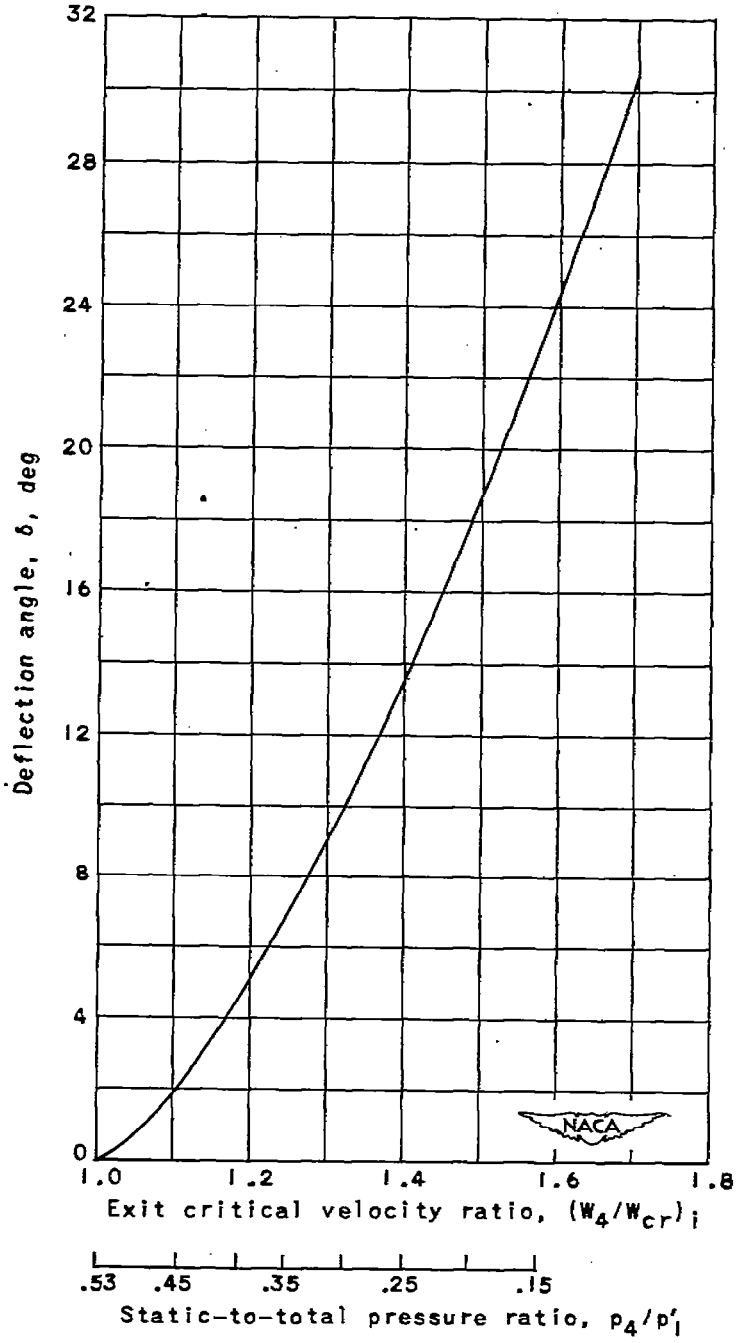

Figure 8. – Variation of deflection angle with exit critical velocity ratio for Method 4 assuming deflection toward axial direction according to Prandtl-Meyer theory of flow around a corner. $\gamma = 1.4$.

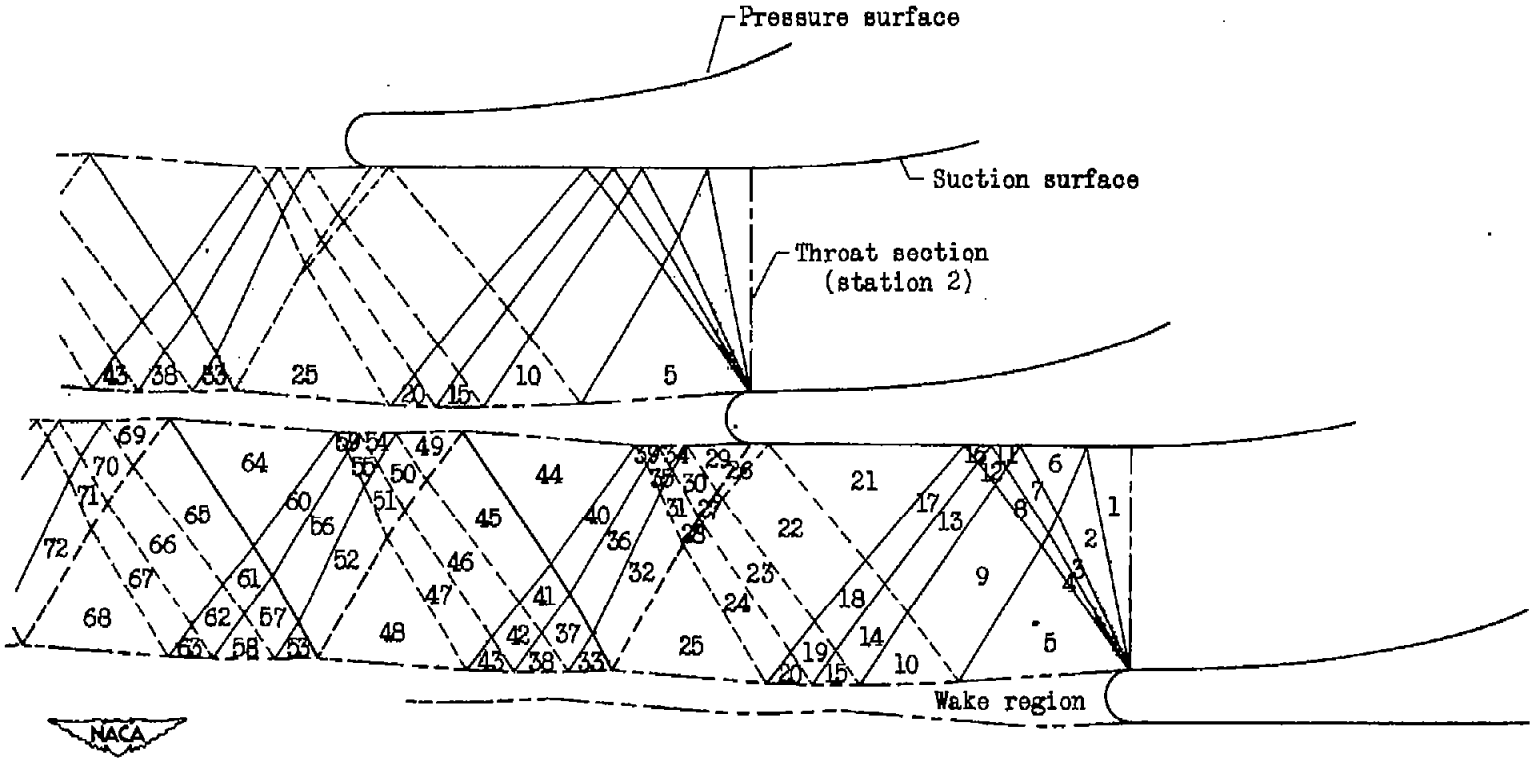

Figure 9. - Diagram of flow conditions at exit of cascade of turbine rotor blades at static-to-total pressure ratio of 0.400 for Method 5, as determined by method of characteristics, assuming downstream static pressure throughout wake region and no separation of flow from suction surface of blade. (See table 1 for flow conditions.)

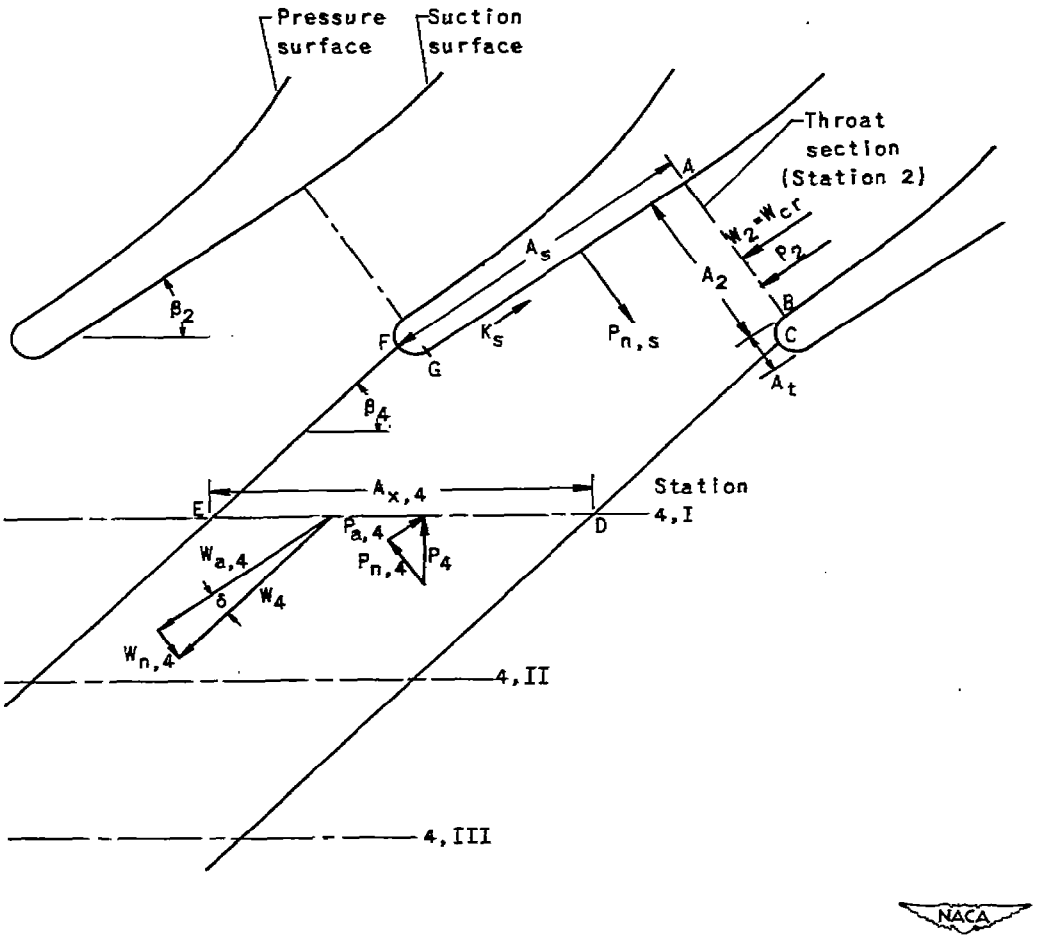

Figure 10. – Diagram of flow conditions at exit of cascade of turbine rotor blades at supercritical pressure ratios for analysis by Method 6, using conservation-of-momentum principle and measured values of static-pressure distribution.

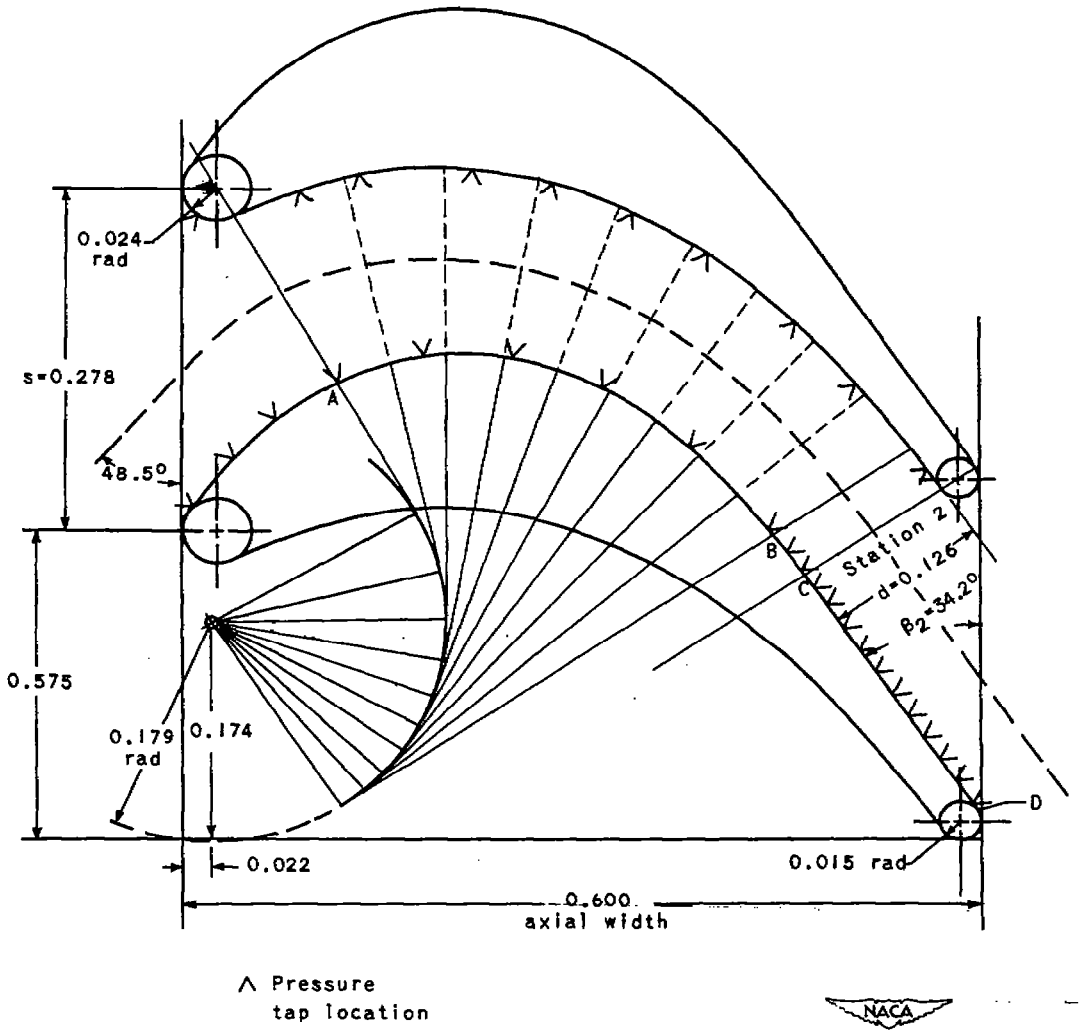

Figure 11. - Blade design used in experimental investigation.
(All dimensions in in.)

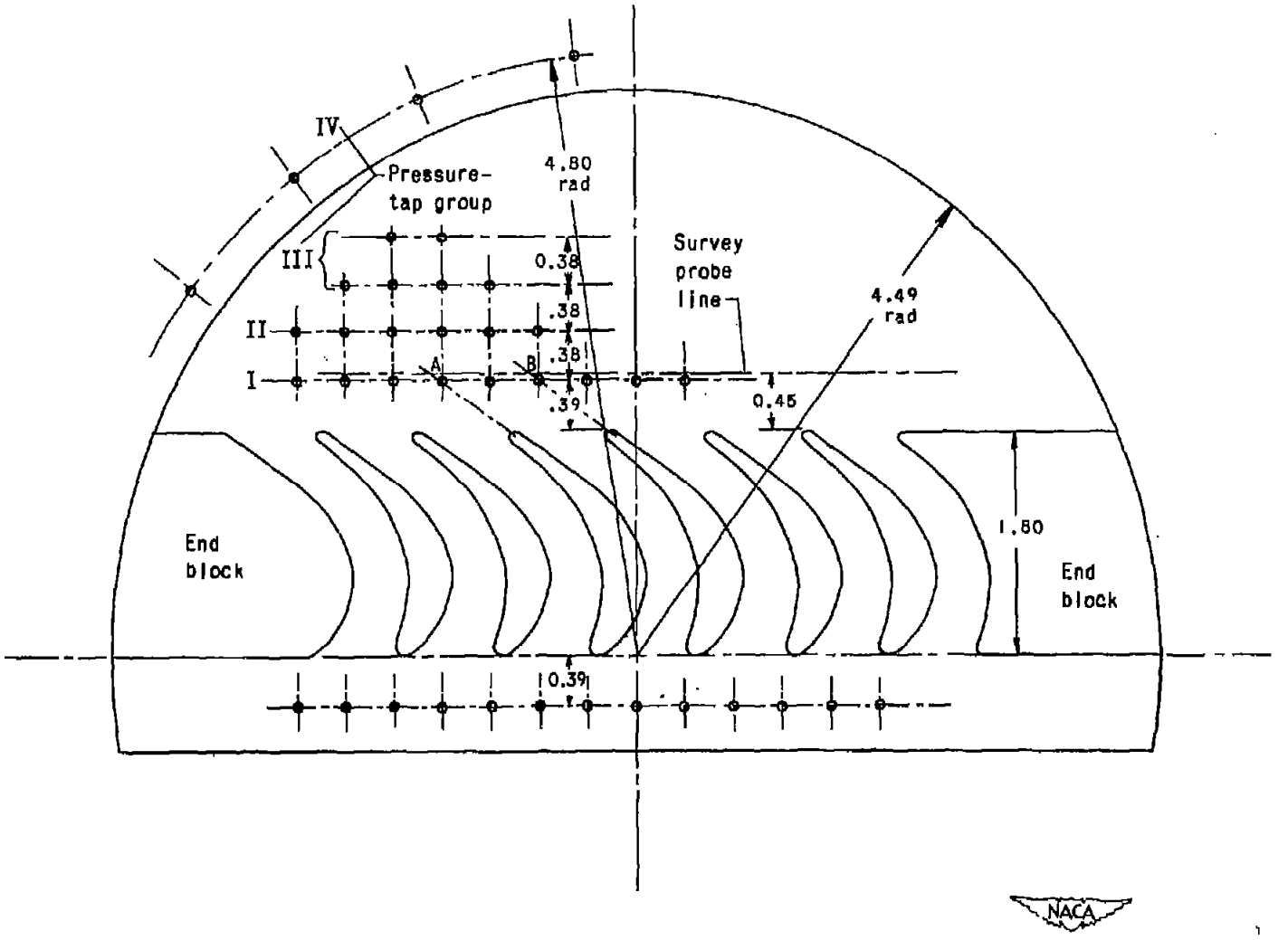

Figure 12. - Plan view of pressure survey blading configuration with top plate removed. (All dimensions in in.)

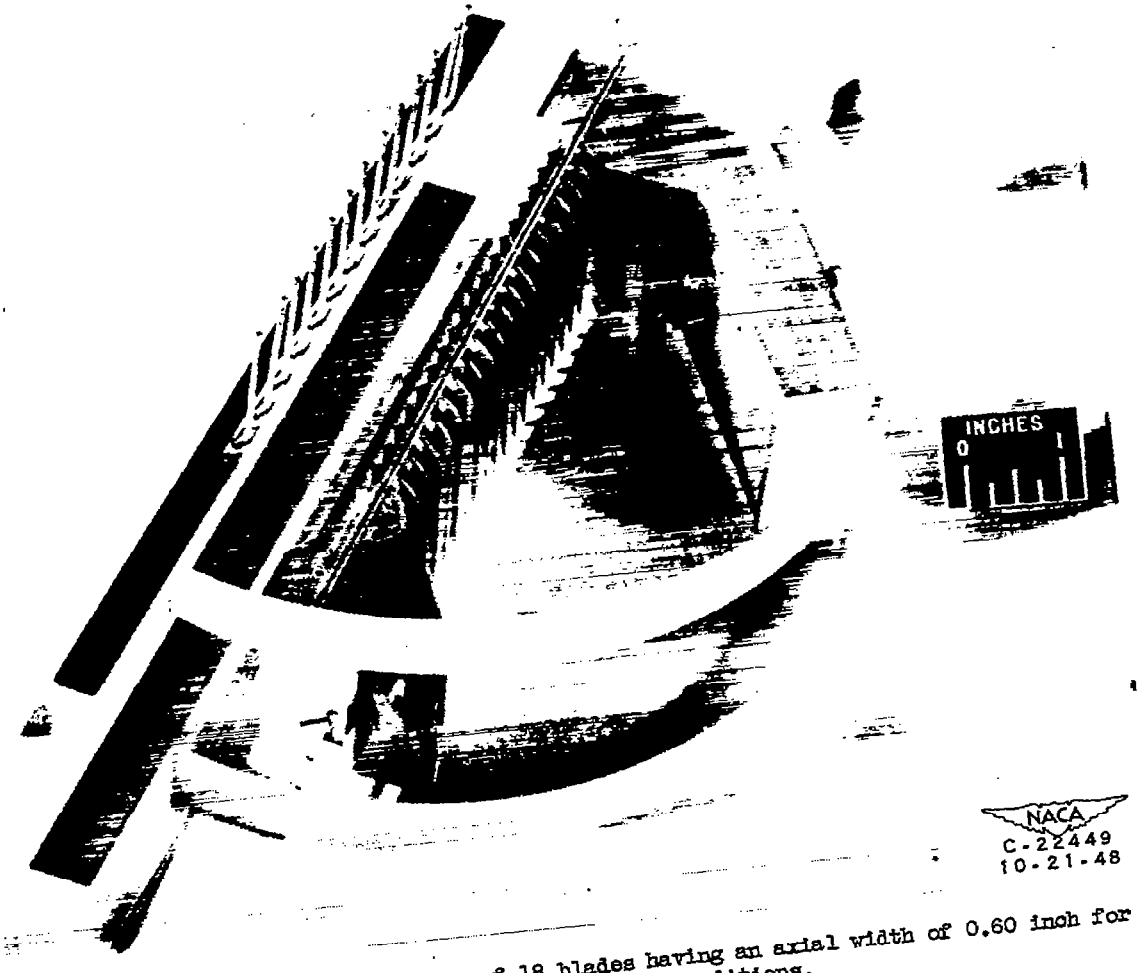

Figure 13. - Cascade configuration of 18 blades having an axial width of 0.60 inch for visual observation of flow conditions.

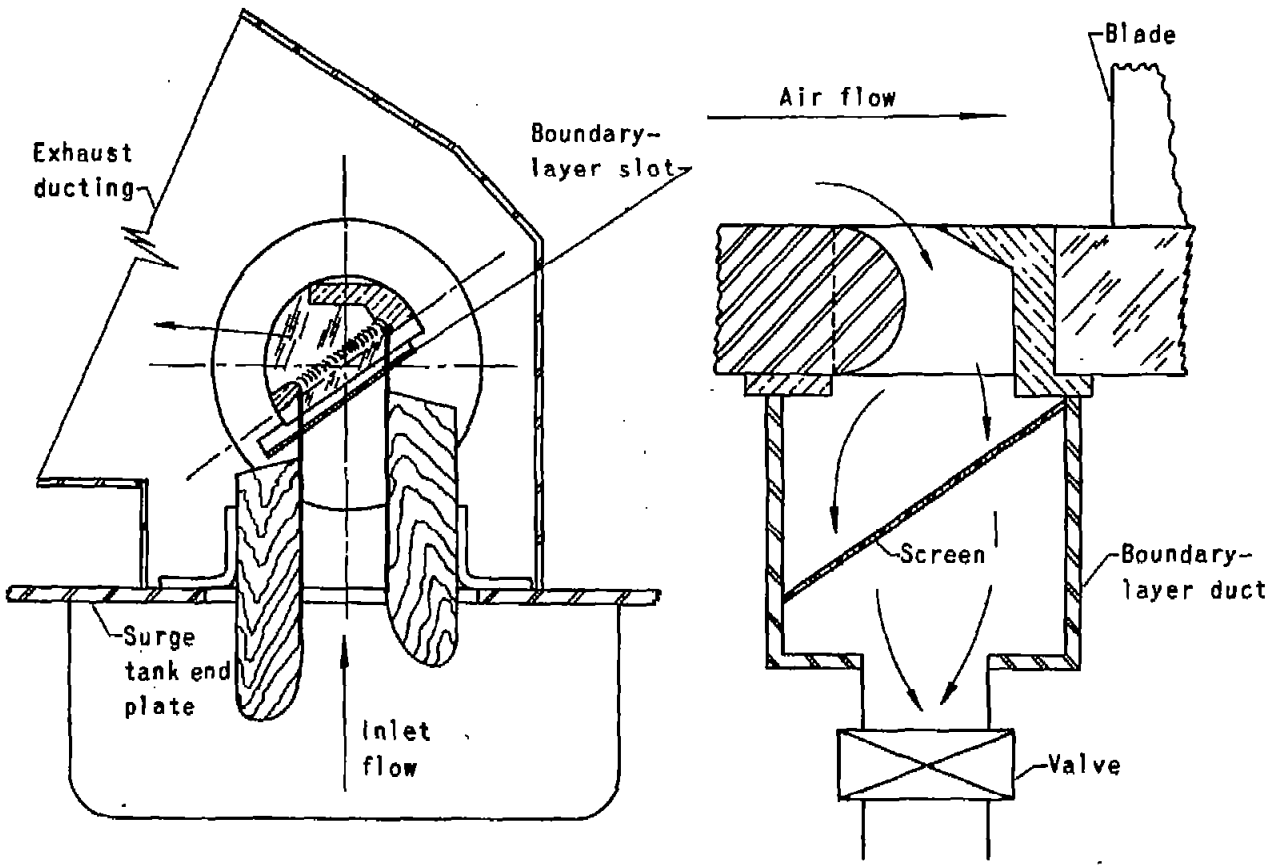

(a) Plan view of cross section through over-all test section assembly.

(b) Detail of boundary-layer removal system.

Figure 14. - Over-all test section assembly and cross section of boundary-layer removal duct.

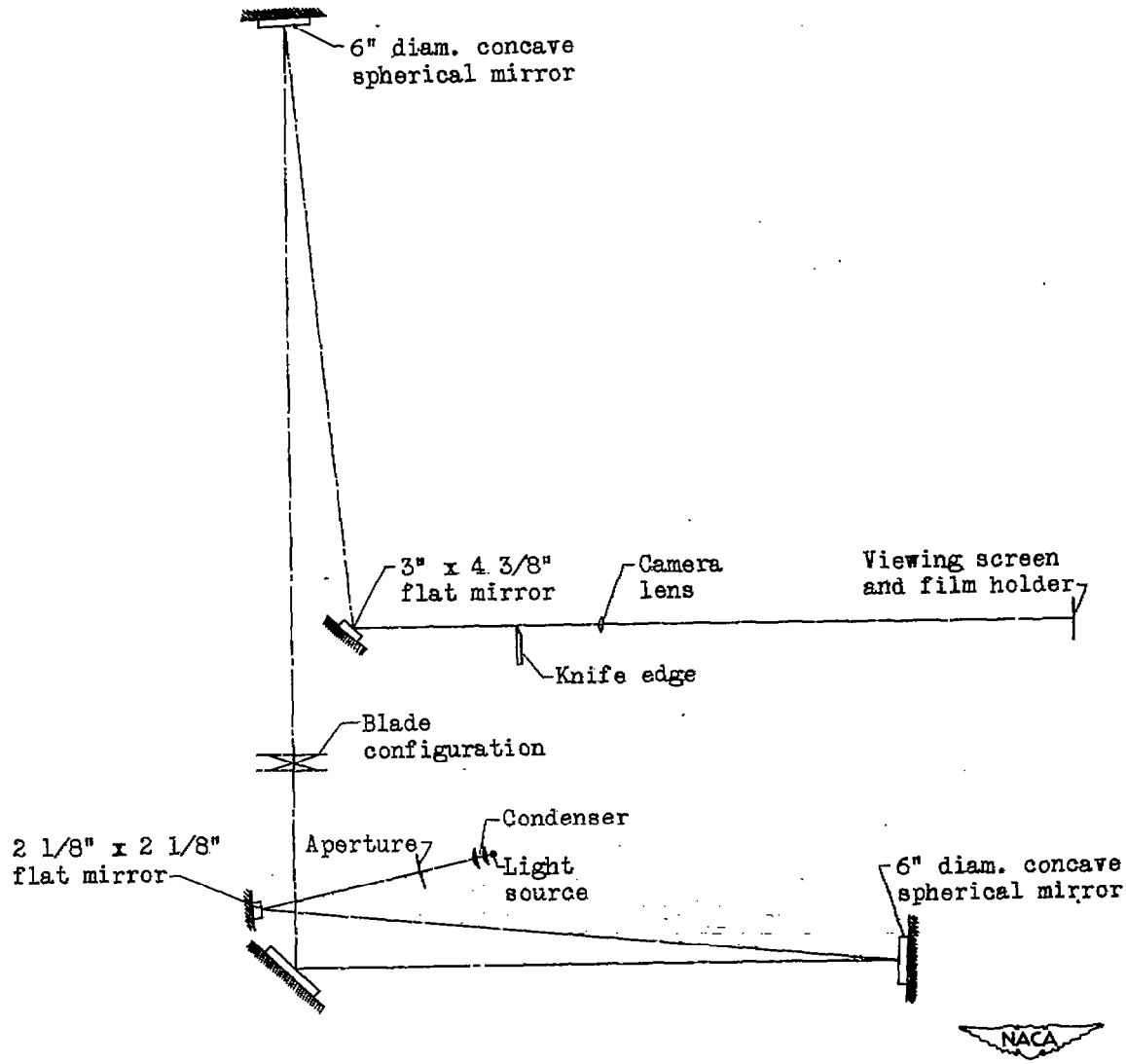

Figure 15. - Diagram of schlieren optical system.

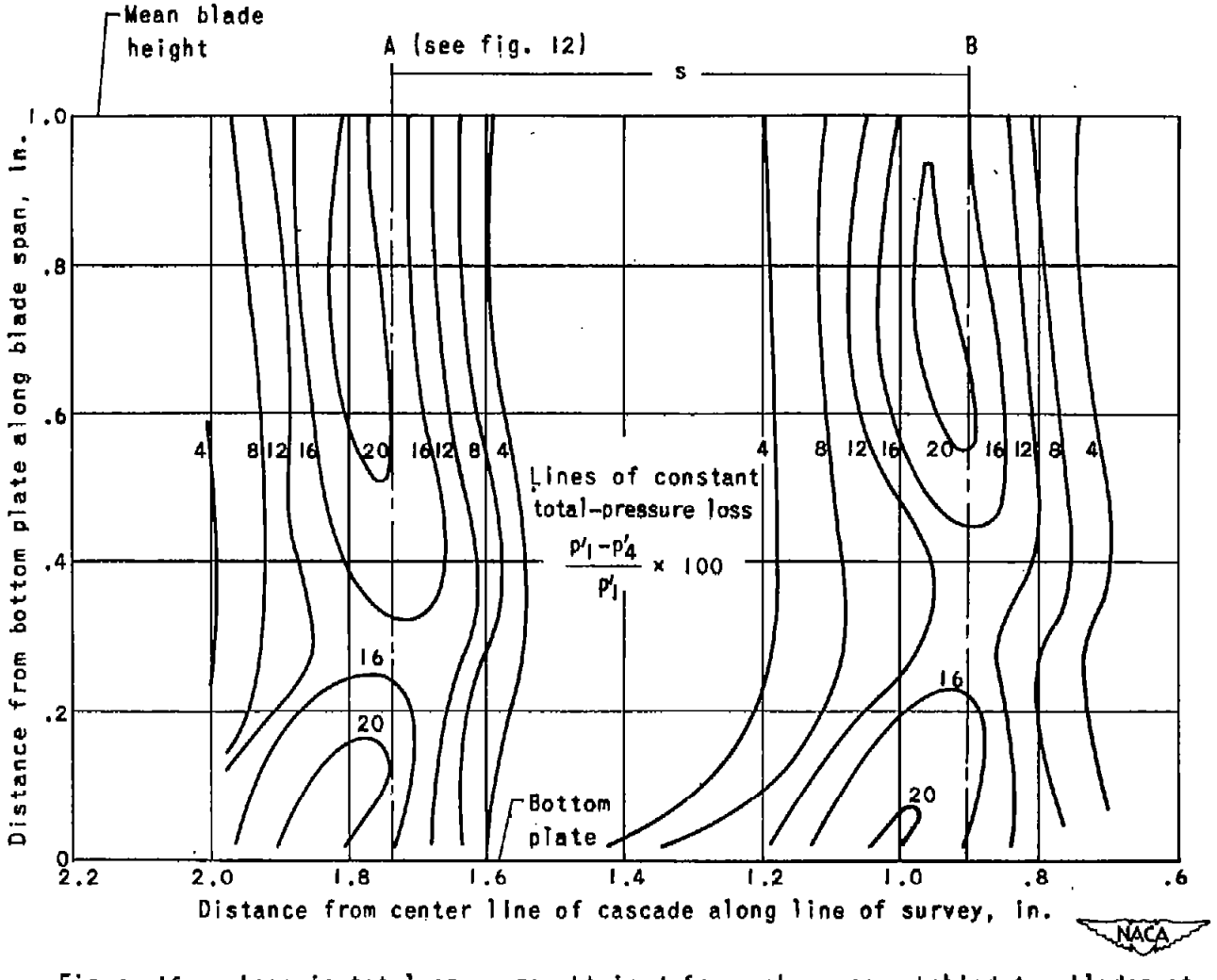

Figure 16. – Loss in total pressure obtained from wake survey behind two blades at an over-all static-to-total pressure ratio of 0.60.

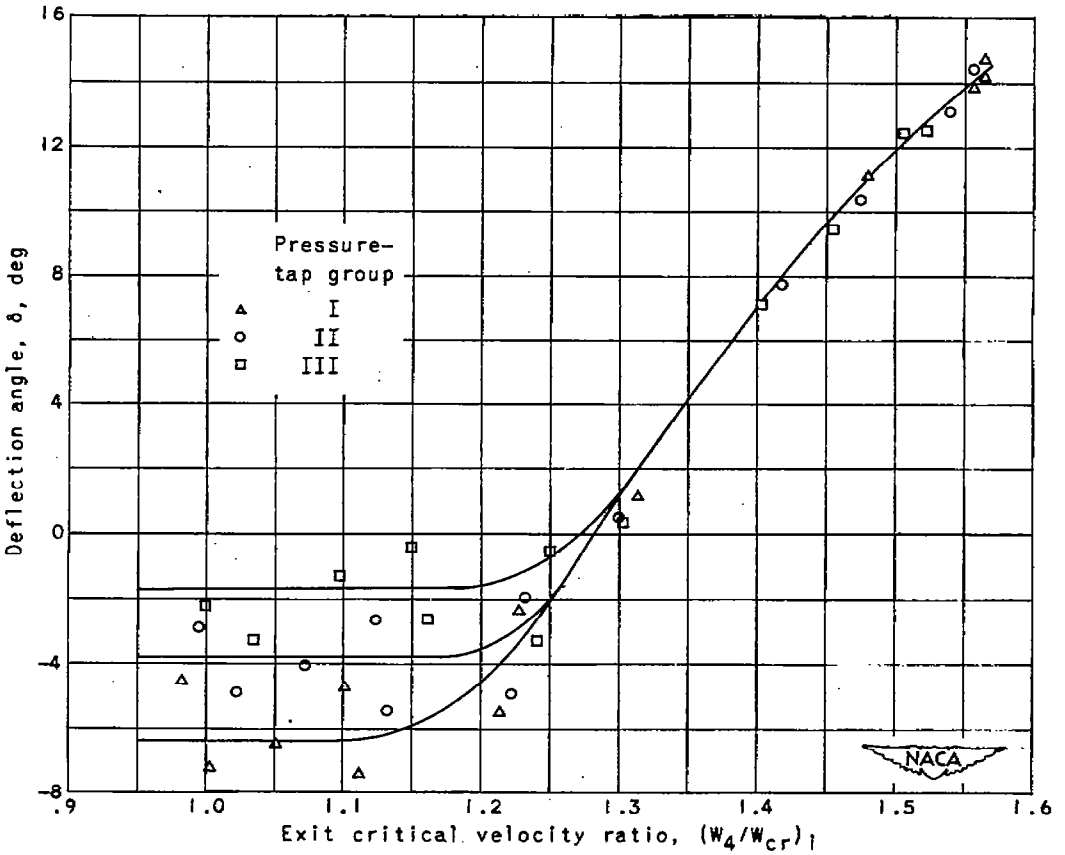

Figure 17. - Experimental evaluation of deflection angle by conservation-of-momentum relationships of Method 6.

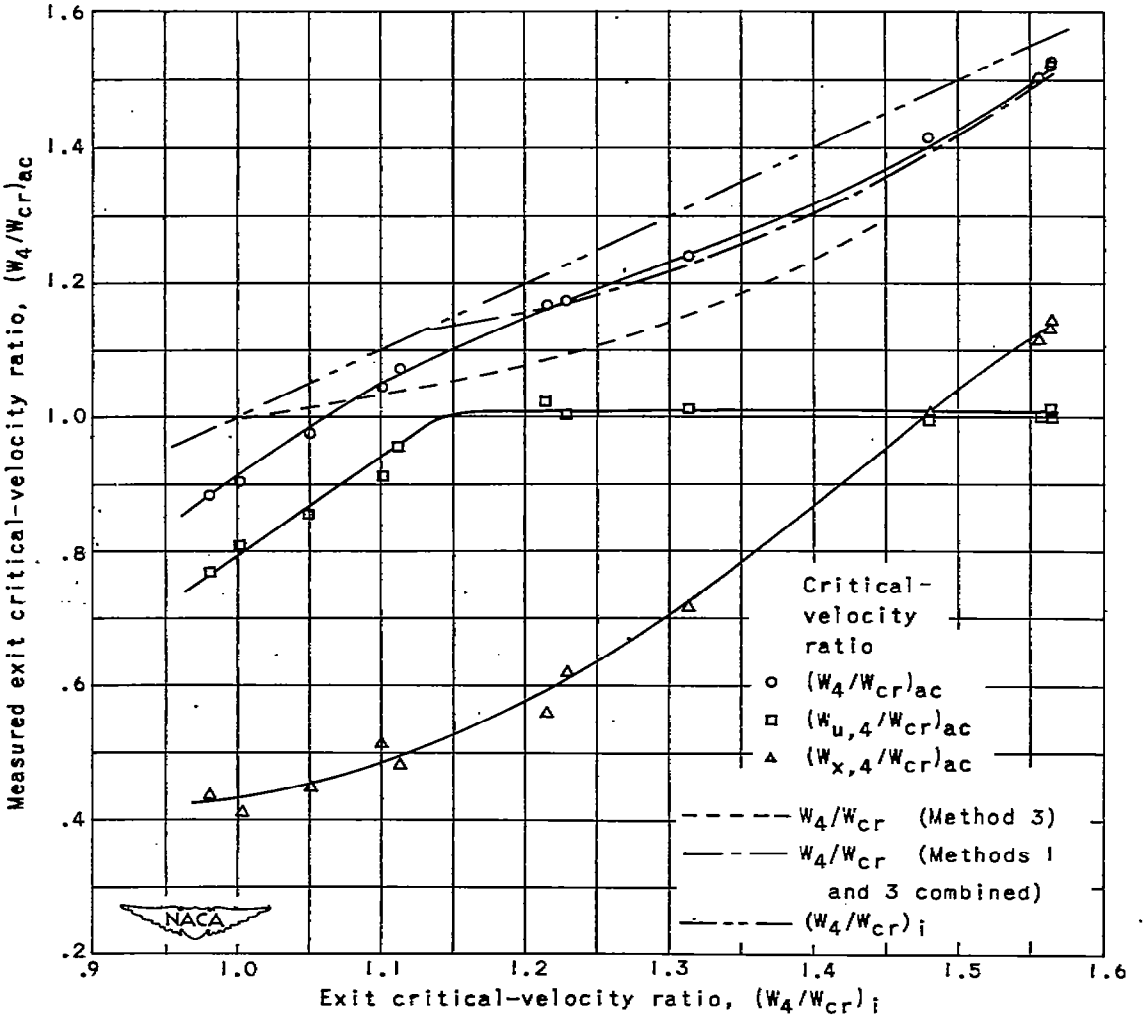

Figure 18. – Experimental evaluation of actual critical-velocity ratio $(W_4/W_{cr})_{ac}$ and components $(W_{u,4}/W_{cr})_{ac}$ and $(W_{x,4}/W_{cr})_{ac}$ by conservation-of-momentum relations of method 6.

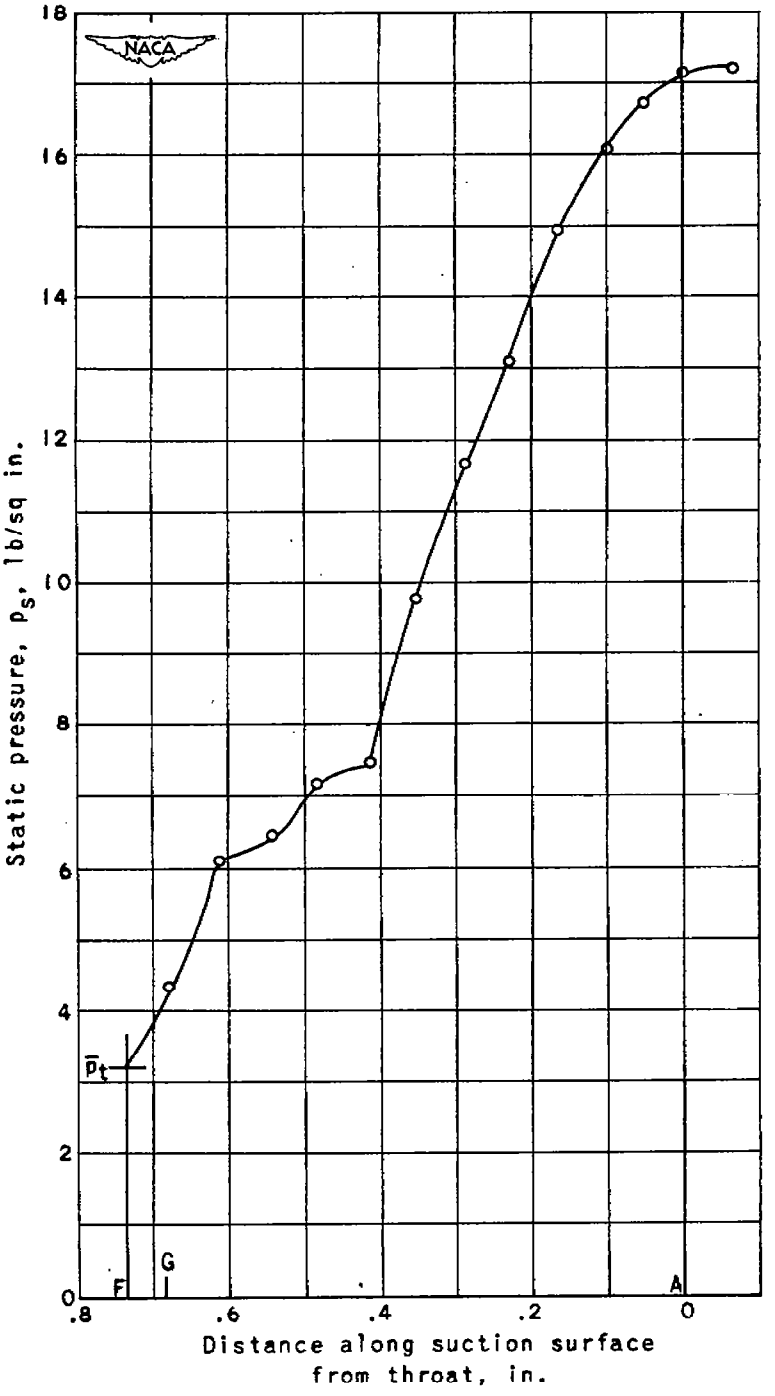

Figure 19. – Static-pressure distribution on suction surface area A_s at point of maximum loading. Area under curve = 7.63 pounds per inch.

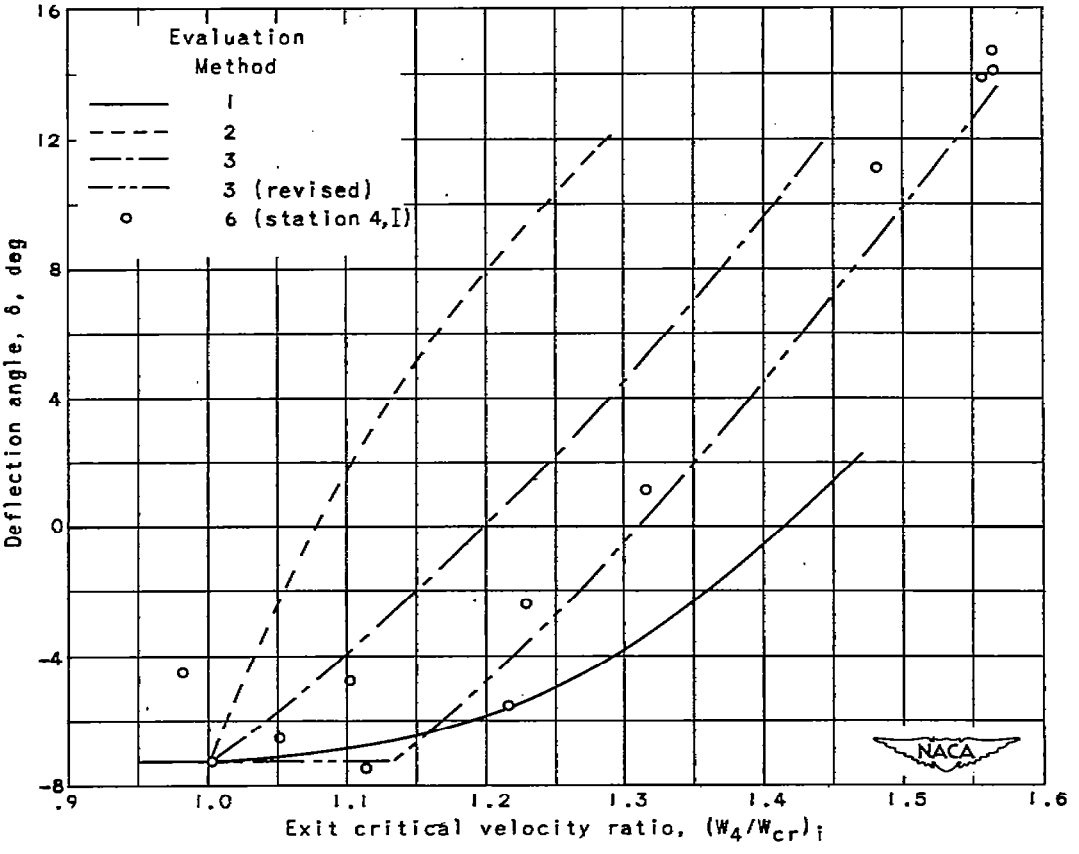

Figure 20. – Comparison of results of evaluation of flow-deflection angle δ by Methods 1, 2, 3, and 6.

(a) Pressure ratio p_4/p'_1, 0.66.

Figure 21. - Schlieren photographs of flow through cascade of 1.80-inch blades with schlieren knife edge parallel to inlet-flow direction.

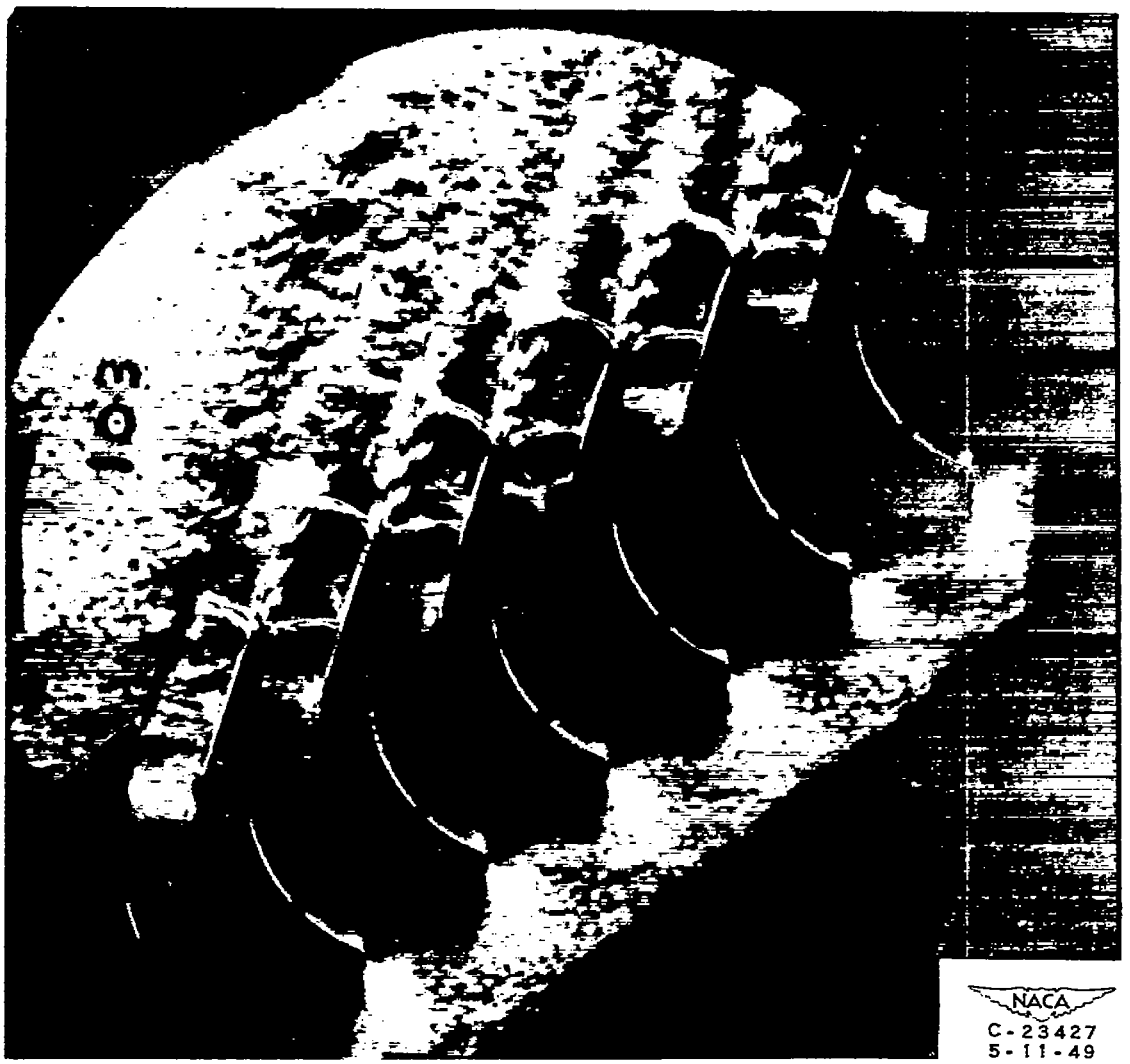

(b) Pressure ratio p_4/p'_1, 0.52.

Figure 21. - Continued. Schlieren photographs of flow through cascade of 1.80-inch blades with schlieren knife edge parallel to inlet-flow direction.

(c) Pressure ratio p_4/p'_1, 0.42.

Figure 21. - Concluded. Schlieren photographs of flow through cascade of 1.80-inch blades with schlieren knife edge parallel to inlet-flow direction.

Figure 22. - Enlargement of schlieren photograph of flow in exit region through two passages of 1.80-inch blades with schlieren knife edge parallel to flow direction. Pressure ratio p_4/p'_1, 0.42.

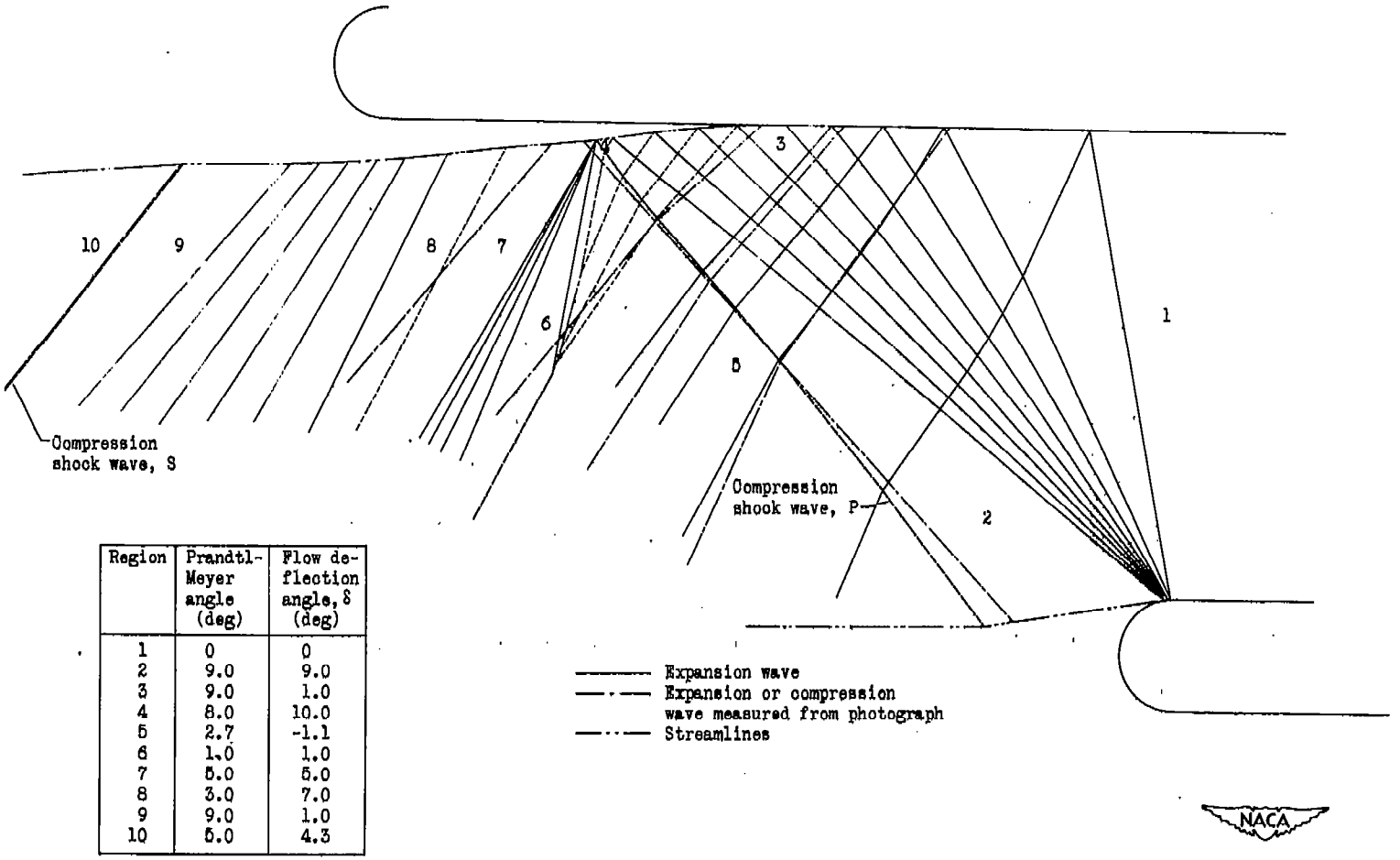

Region	Prandtl-Meyer angle (deg)	Flow deflection angle, δ (deg)
1	0	0
2	9.0	9.0
3	9.0	1.0
4	8.0	10.0
5	2.7	-1.1
6	1.0	1.0
7	5.0	5.0
8	3.0	7.0
9	9.0	1.0
10	5.0	4.3

Figure 23. - Diagram of flow conditions at exit of cascade as evaluated from schlieren photograph of figure 22 using method of characteristics. Pressure ratio, $p_4/p_1' = 0.42$.

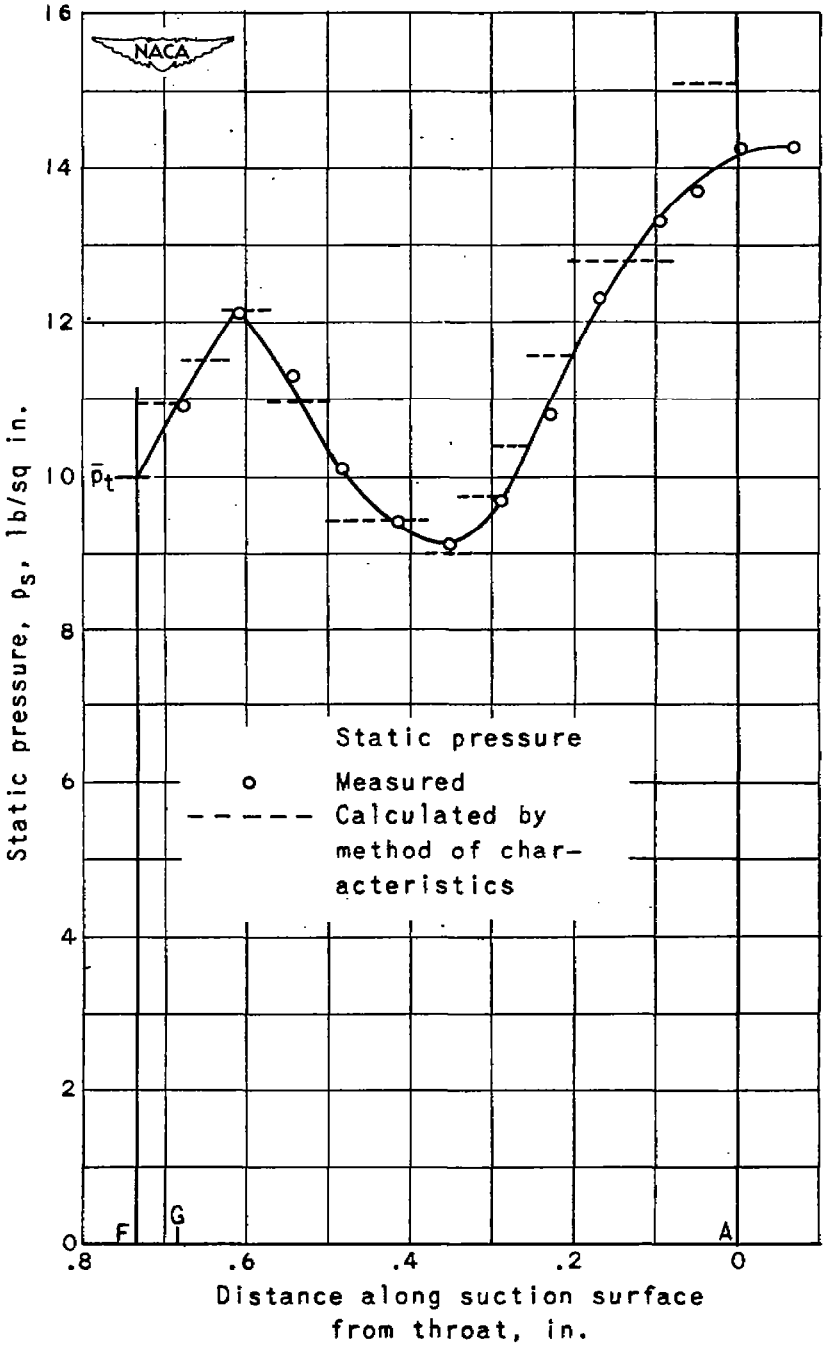

Figure 24. - Static-pressure distribution on suction surface area A_s for condition shown in schlieren photograph of figure 22. Pressure ratio, $p_4/p_1' = 0.42$.

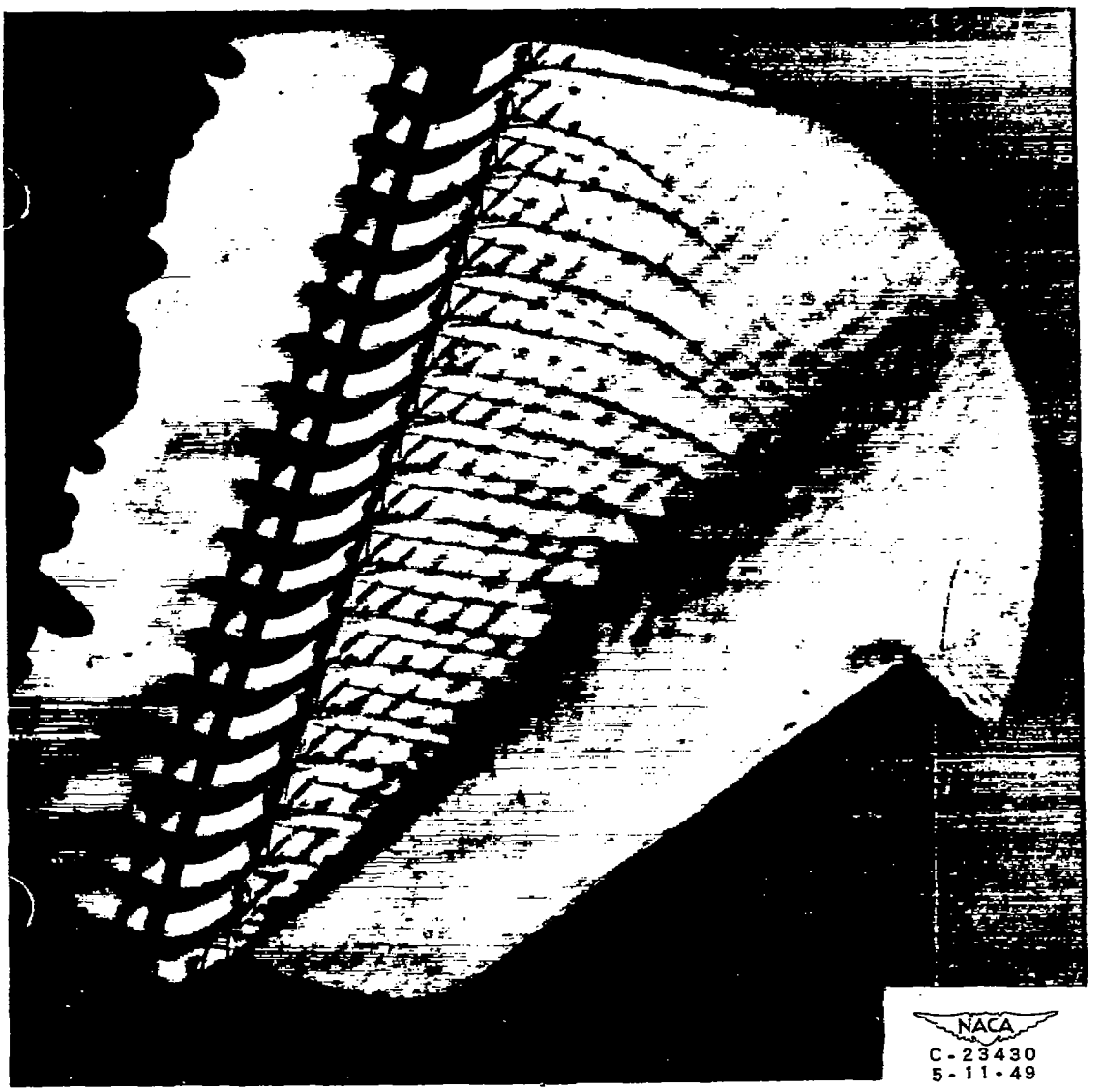

(a) Schlieren knife edge parallel to flow direction in exit region; pressure ratio p_4/p'_1, 0.44.

Figure 25. - Photographs of flow through cascade of 0.60-inch blades.

(b) Shadowgraph; pressure ratio p_4/p'_1, 0.39.

Figure 25. - Continued. Photographs of flow through cascade of 0.60-inch blades.

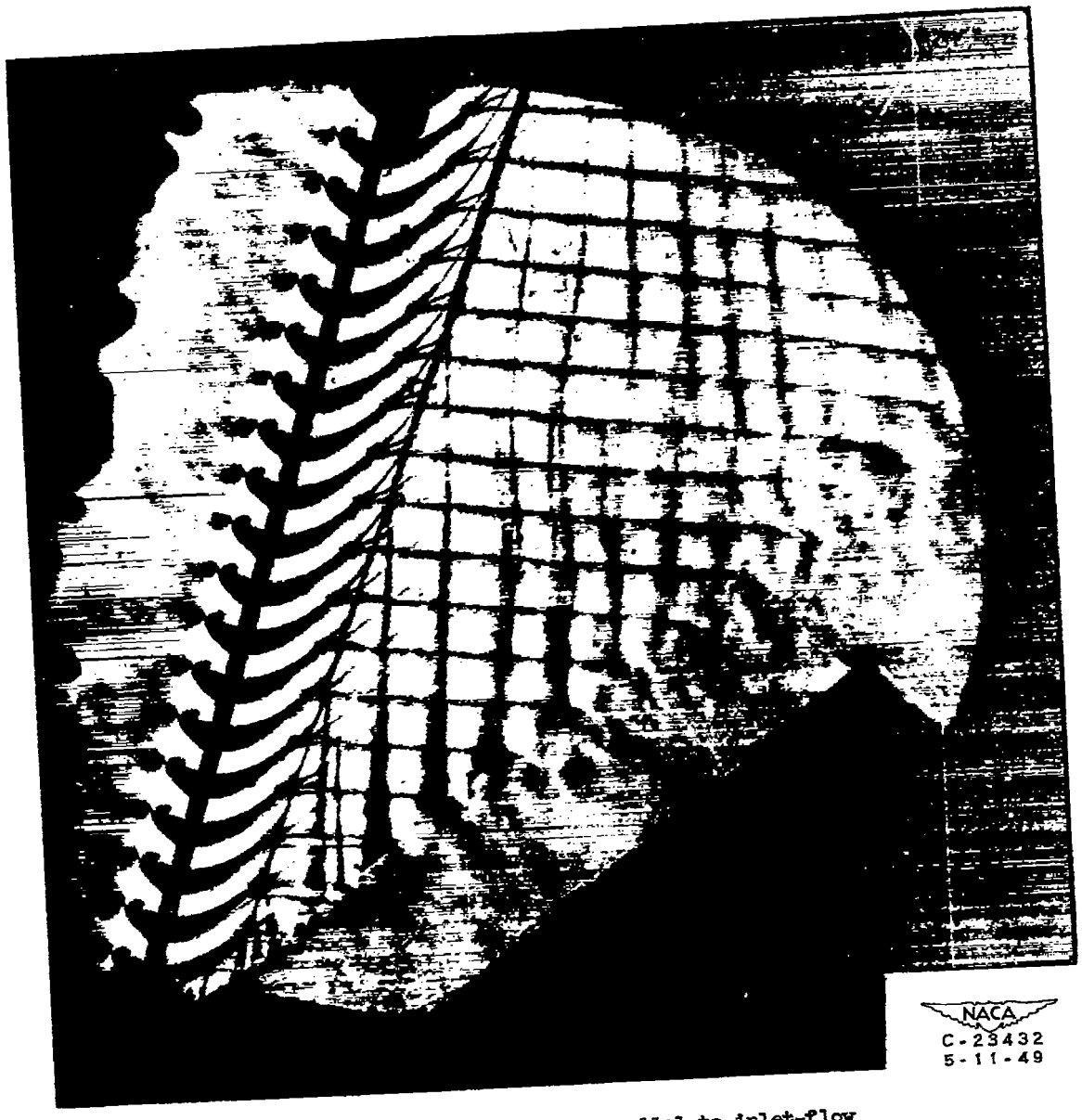

(c) Schlieren knife edge parallel to inlet-flow direction; pressure ratio P_4/P'_1, 0.25.

Figure 25. - Continued. Photographs of flow through cascade of 0.60-inch blades.

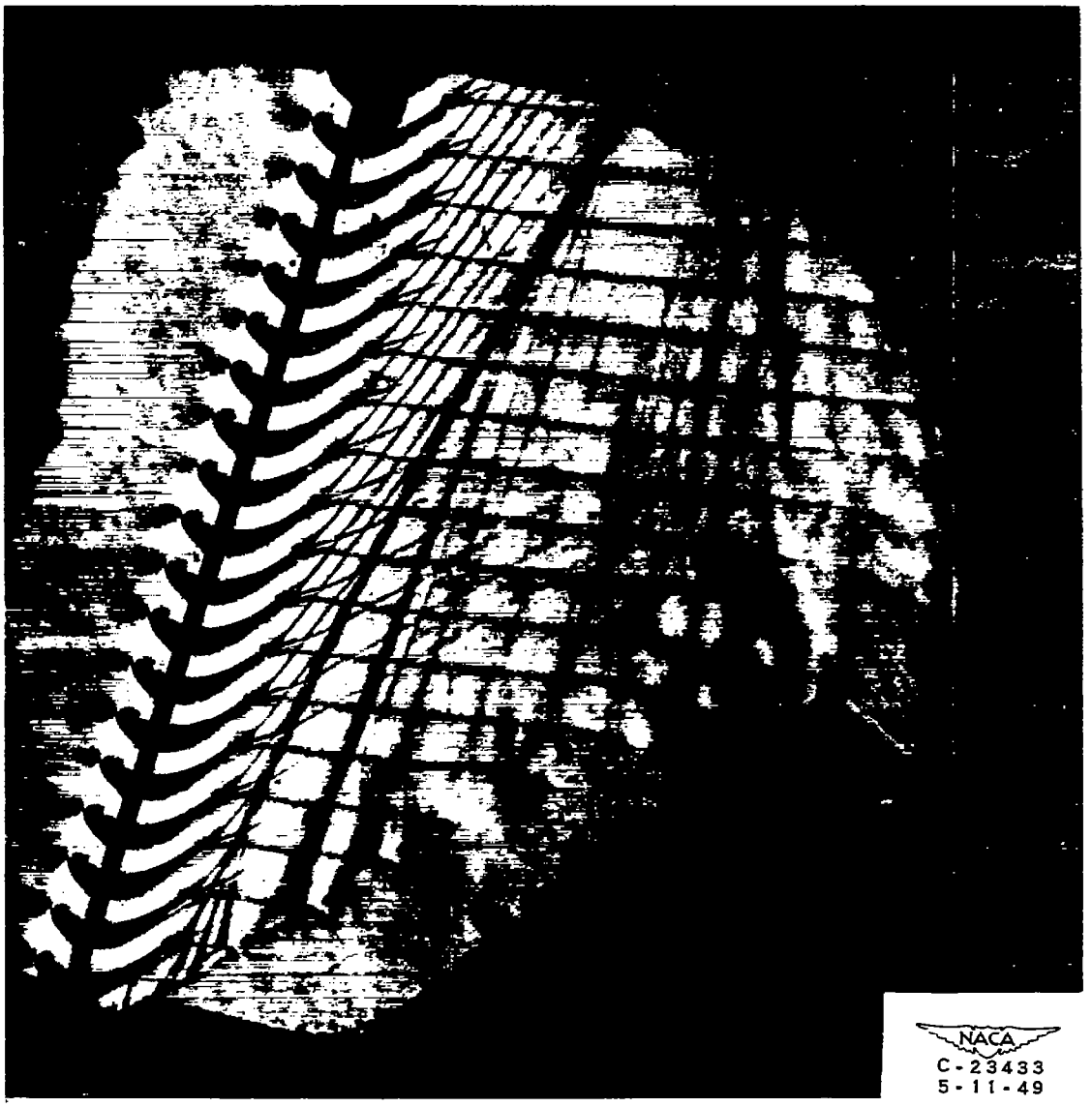

(d) Schlieren knife edge parallel to inlet-flow direction; pressure ratio p_4/p'_1, 0.21.

Figure 25. - Concluded. Photographs of flow through cascade of 0.60-inch blades.

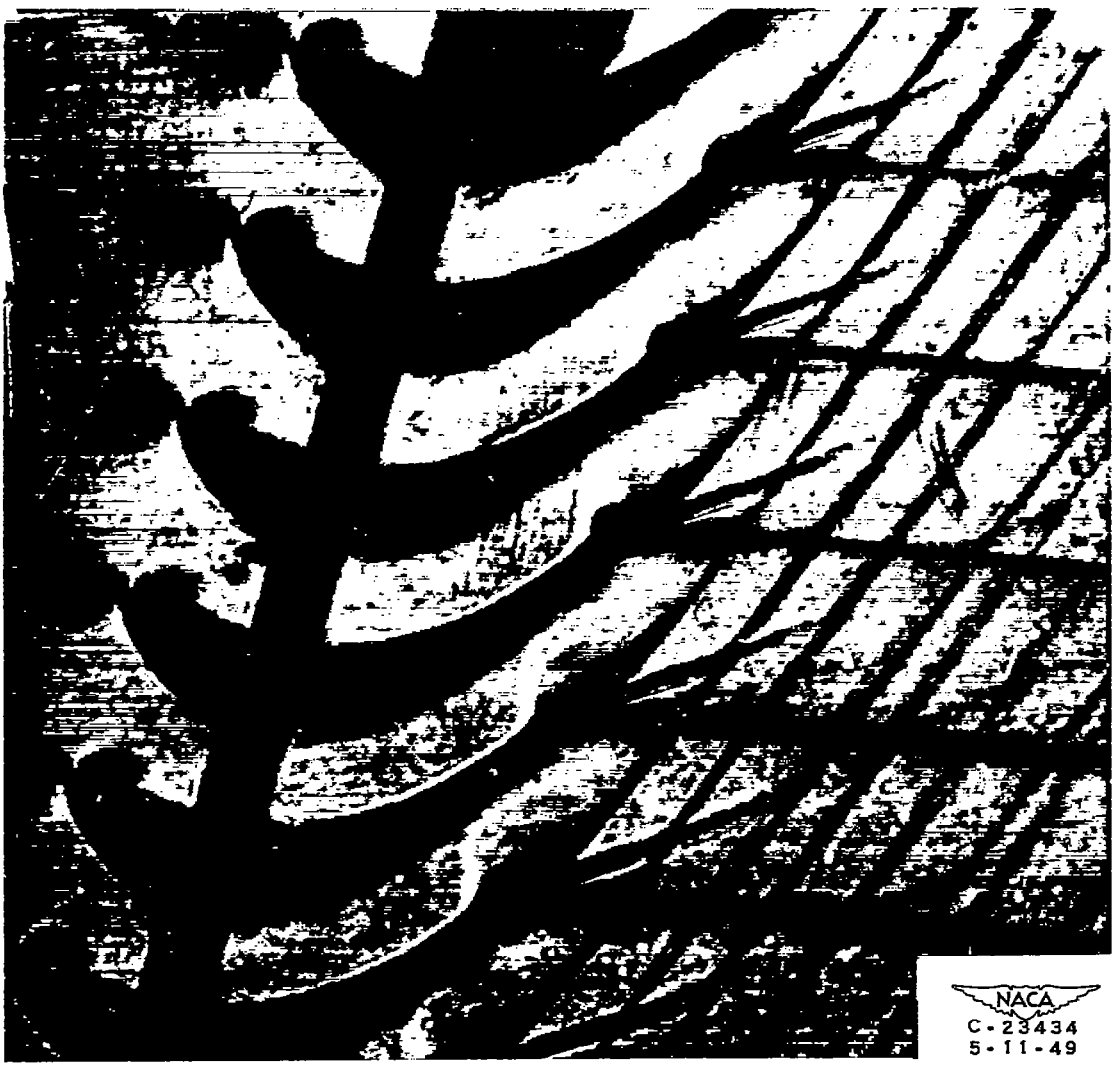

Figure 26. - Enlargement of schlieren photograph of flow through passages of 0.60-inch blades with schlieren knife edge parallel to inlet-flow direction. Pressure ratio p_4/p'_1, 0.23.

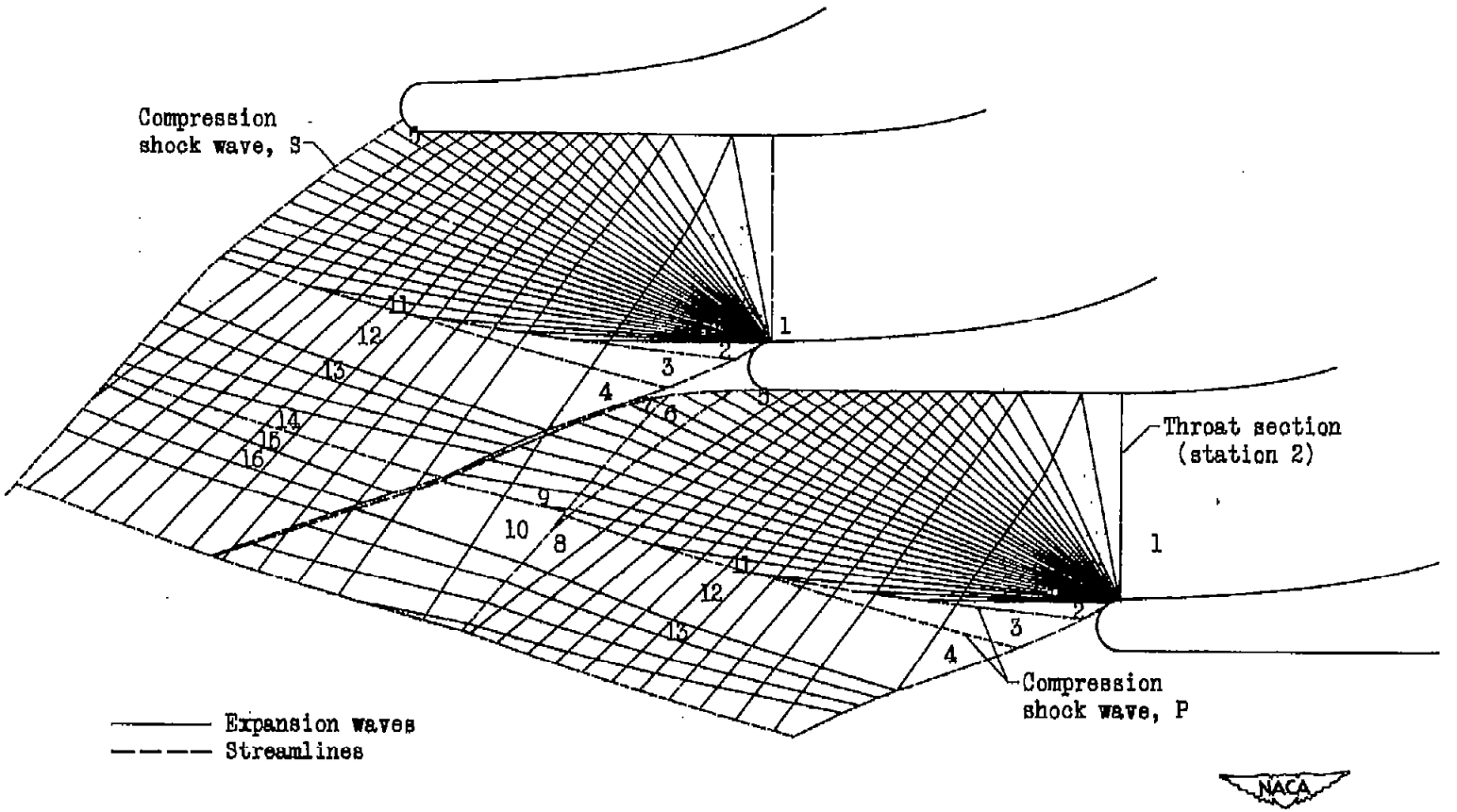

Figure 27. - Diagram of flow conditions at exit of cascade evaluated from schlieren photograph of figure 26 using method of characteristics. Pressure ratio, $p_4/p'_1 = 0.23$. (See table 2 for flow conditions.)